AEDC-TR-73-106

SEP 5 1973
OCT 1 1973

LAMINAR HEAT TRANSFER ON SHARP AND BLUNT TEN-DEGREE CONES IN CONICAL AND PARALLEL LOW-DENSITY FLOW

D. E. Boylan

ARO, Inc.

August 1973

VON KÁRMÁN GAS DYNAMICS FACILITY
ARNOLD ENGINEERING DEVELOPMENT CENTER
AIR FORCE SYSTEMS COMMAND
ARNOLD AIR FORCE STATION, TENNESSEE

NOTICES

When U. S. Government drawings specifications, or other data are used for any purpose other than a definitely related Government procurement operation, the Government thereby incurs no responsibility nor any obligation whatsoever, and the fact that the Government may have formulated, furnished, or in any way supplied the said drawings, specifications, or other data, is not to be regarded by implication or otherwise, or in any manner licensing the holder or any other person or corporation, or conveying any rights or permission to manufacture, use, or sell any patented invention that may in any way be related thereto.

Qualified users may obtain copies of this report from the Defense Documentation Center.

References to named commercial products in this report are not to be considered in any sense as an endorsement of the product by the United States Air Force or the Government.

LAMINAR HEAT TRANSFER ON SHARP AND BLUNT TEN-DEGREE CONES IN CONICAL AND PARALLEL LOW-DENSITY FLOW

D. E. Boylan
ARO, Inc.

FOREWORD

The research reported herein was conducted at the Arnold Engineering Development Center (AEDC) under Program Element 64719F.

The results of tests presented were obtained by ARO, Inc. (a subsidiary of Sverdrup & Parcel and Associates, Inc.), contract operator of AEDC, Air Force Systems Command (AFSC), Arnold Air Force Station, Tennessee.

The experiments were conducted from March through April, 1971, under ARO Project No. VT2166, and supplemental data were obtained from March 13 to April 7, 1972, under ARO Project No. VM2266. The manuscript was submitted for publication on April 23, 1973.

The results reported herein have been made possible by the extensive development of heat-transfer instrumentation by C. T. Kidd of the VKF Aerodynamics Division Instrumentation Branch.

A sharp cone correlation technique developed herein follows a procedure suggested by Dr. W. S. Norman of the VKF Aerodynamic Projects Branch. The correction procedure for source flow effects utilizes the unpublished development of D. A. Wagner of the VKF Aerodynamic Projects Branch.

This technical report has been reviewed and is approved.

JOHN R. TAYLOR
Major, USAF
Chief, Research and Development Division
Directorate of Technology

ROBERT O. DIETZ
Director of Technology

ABSTRACT

The report presents heat-transfer-rate measurements on sharp and blunt 10-deg half-angle cones at angles of attack between -9 and +10 deg in a low-density, hypersonic wind tunnel. Circumferential and longitudinal distributions are presented for cold wall conditions at $18.2 \leq M_\infty \leq 19.9$ and $960 \leq Re_\infty/in. \leq 1250$. The effect of source-like flows was studied by utilizing both conical and contoured expansion nozzles with the same free-stream similarity parameters and model wall temperatures. Comparisons are made to previously published experimental and theoretical results.

CONTENTS

ILLUSTRATIONS

APPENDIX
TABLES

NOMENCLATURE

A^*	Sonic area
C_e^*	Chapman-Rubensin constant based on local inviscid boundary-layer edge conditions (Eq. 12)
C_∞^*	Chapman-Rubensin constant (Eq. 4)
C_1	Constant in Eq. (1)
d	Nose diameter
E_o	Heat-transfer gage output
H_{aw}	Adiabatic wall enthalpy
H_e	Enthalpy based on local inviscid edge conditions
H_o	Stagnation enthalpy
H_w	Wall enthalpy
H_*	Reference enthalpy (Eq. 13)
h	Convective heat-transfer coefficient (Eq. 2)
K	Cheng's thin shock layer parameter, $p_\infty R_N/\mu_\infty U_\infty C_\infty^*$
K'	Constant in Eq. (11)

k	Nose drag coefficient (0.964 for spherically blunted cone)
L_{max}	Maximum model length
L_s	Distance from apparent source of nozzle flow to model nose
ℓ	Sharp cone slant length to instrumentation station
M_∞	Free-stream Mach number
$\dot{m}$	Mass flow rate
Pr	Prandtl number
p_e	Local inviscid edge pressure
p_o	Stagnation pressure
p_o'	Free-stream stagnation pressure
p_∞	Free-stream static pressure
$\dot{q}$	Heat-transfer rate
$\dot{q}_o$	Heat-transfer rate at the stagnation point
q_∞	Free-stream dynamic pressure
Re_2	Unit Reynolds number downstream of a normal shock
Re_∞	Free-stream unit Reynolds number
$Re_{\infty,d}$	Free-stream Reynolds number based on nose diameter
$Re_{\infty,x'}$	Free-stream Reynolds number based on x'
$Re_{e,\ell}$	Reynolds number based on inviscid boundary-layer edge conditions and cone slant length ℓ
R_B	Model base radius
R_N	Model nose radius
S	Surface distance measured from model stagnation point
S_∞	Free-stream speed ratio, $U_\infty/(2RT_\infty)^{1/2}$
S_t	Free-stream Stanton number, $\dot{q}/\rho_\infty U_\infty(H_o - H_w)$
$\bar{S}_t$	Free-stream Stanton number for an equivalent uniform flow field
$S_{t_{e,aw}}$	Stanton number based on local inviscid edge conditions and adiabatic wall enthalpy, $\dot{q}/\rho_e U_e(H_{aw} - H_w)$
S_{t_o}	Stagnation point Stanton number, $\dot{q}_o/\rho_\infty U_\infty (H_o - H_w)$

T_G	Gas local temperature
T_∞	Free-stream static temperature
T_O	Stagnation temperature
T_W	Wall temperature
T_*	Reference temperature (Eq. 5 for blunt cones and Eq. 7 or 13 for sharp cones)
U_∞	Free-stream velocity
U_e	Local inviscid edge velocity
$\bar{V}_*$	Similarity parameter defined for blunt cones by Eq. 3 and for sharp cones by Eq. 6
x	Distance from nozzle exit measured on tunnel centerline
x'	Axial distance from model nose to instrumentation station
α	Angle of attack
γ	Ratio of specific heats
λ_∞	Free-stream mean free path
ϵ	$(\gamma - 1)/(\gamma + 1)$
θ_C	Cone half-angle
μ_∞	Free-stream viscosity
μ_*	Viscosity at reference temperature T_*
ξ	Conical flow parameter x'/L_S
ρ_e	Local inviscid boundary-layer edge density
ρ_∞	Free-stream density
ϕ	Model ray angle, $\phi = 0$ is windward for positive angle of attack and leeward for negative angle of attack

SECTION I
INTRODUCTION

Hypersonic wind tunnels may employ heaters ranging from conventional electric-resistance types to continuous or intermittent arc-discharge devices. The resulting real gas nonequilibrium phenomena sometimes introduce a degree of uncertainty when wind tunnel results are being analyzed. In addition to these problems, nonuniform flow induced when conical expansion nozzles are used introduces difficulties in data interpretation. A cooperative program involving Deutsche Forschungs-Und Versuchsanstalt Für Luft-Und Raumfahrt (DFVLR), Air Force Flight Dynamics Laboratory (AFFDL), and the AEDC was designed to study this problem. Facilities at AEDC, AFFDL, Porz-Wahn and Gottingen, Germany, will eventually be utilized to produce pressure and heat-transfer data on standard, 10-deg half-angle, blunt and sharp cones so that comparisons between results from different facilities and analyses of the effects of different flow conditions may be conducted.

The first phase of the AEDC investigation consisted of measurements of heat-transfer rates on sharp and blunt 10-deg cones utilizing both conical and contoured nozzles at approximately the same energy level and degree of flow rarefaction. Hypersonic, arc-heated flows of nitrogen were used.

Although the present investigation was conducted in a low-density facility, a high degree of rarefaction was not desired because that would introduce complications into comparisons between different facilities. The purpose of this report is to describe the experimental results of the surface heat-transfer-rate measurements and make comparisons to published experimental results, as well as some recent data generated at one other facility engaged in the cooperative program. Comparisons are also made to applicable theoretical calculations. A similar report on cone surface pressure measurements is being prepared.

SECTION II
APPARATUS

2.1 TUNNEL M

Tunnel M, where this work was conducted, is shown photographically in Fig. 1a and schematically in Fig. 1b. It is a continuous, arc-heated, low-density, hypersonic wind tunnel normally using nitrogen as the test gas. Pumping is provided by three stages of air ejectors in series which exhaust into the von Karman Facility (VKF) main compressor system through the VKF Tunnel C test section. This arrangement permits simultaneous operation of these two tunnels, or either can be operated alone. Tunnel M consists basically of the following major components, in streamwise order:

1. Rotating-arc-type d-c arc heater with a power supply rated at 200 kw for continuous operation. Gas is injected into the arc heater in a swirl mode.
2. Cylindrical settling chamber of 1.5-in. diam and 3-in. length.
3. Both an axisymmetric, contoured, aerodynamic Mach 18 nozzle and a 14-deg half-angle, conical, expansion nozzle were used in the present study. An additional Mach 12 contoured nozzle is described in Ref. 1.
4. Stationary bulkhead of 94-in. diam which supports the nozzle, probe drive and support unit, pressure measuring system, and external force balance or model support base. The bulkhead contains eight 12-in.-diam ports.
5. Cylindrical 8-ft-diam test chamber which moves downstream to allow access to the test section, models, and probes.
6. Axisymmetric diffuser with convergent entrance, constant area throat, and divergent outlet. Interchangeable units are available for different test configurations.
7. Downstream heat exchanger.
8. First air ejector stage.
9. Isolation valve.

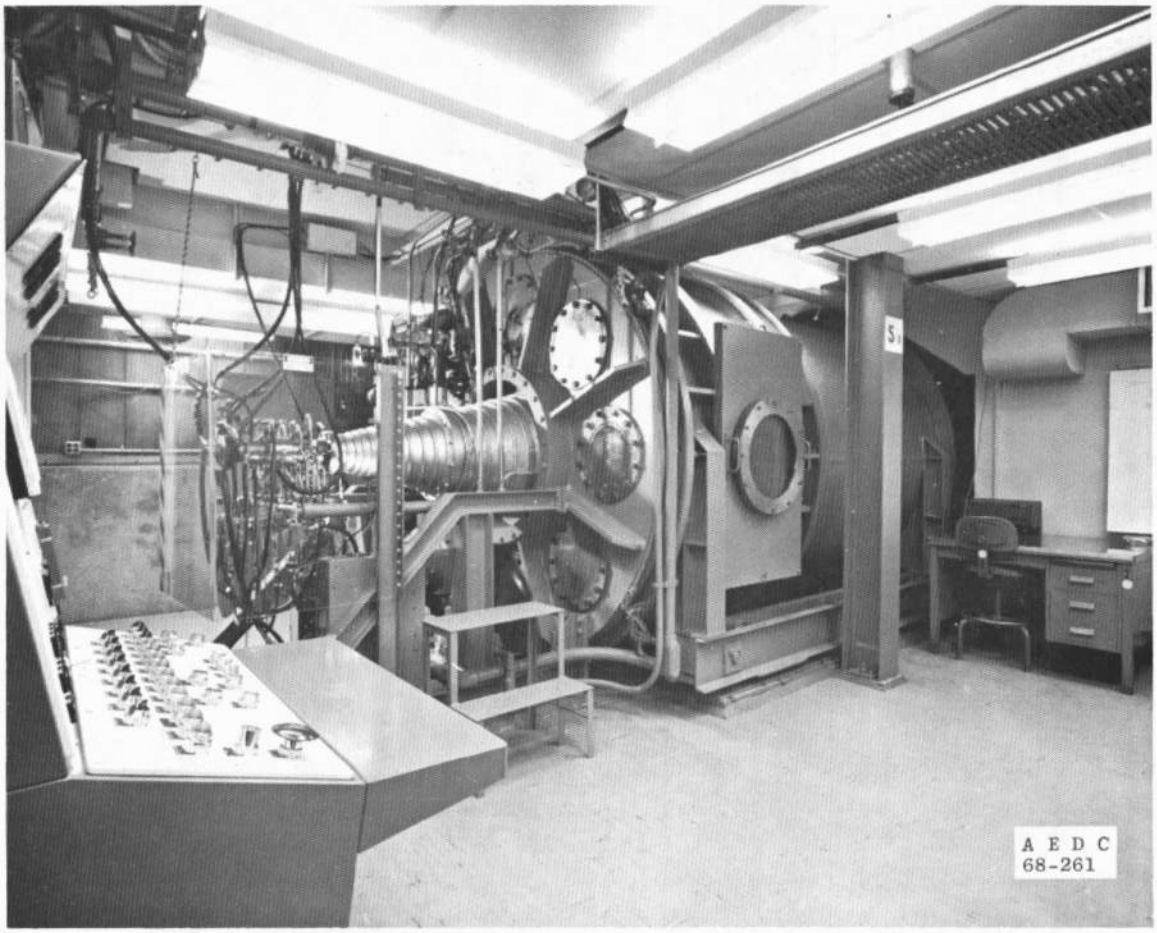

a. Photograph of Tunnel M

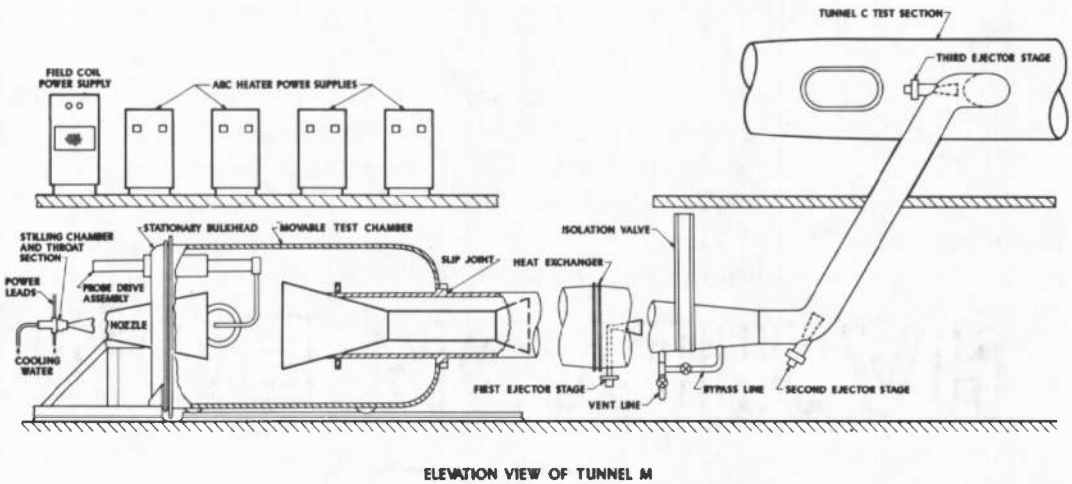

b. Elevation View of Tunnel M

Fig. 1 Tunnel M

2.2 NOZZLE FLOW CONDITIONS

Nozzle free-stream flow conditions are determined by continuous measurements of free-stream stagnation pressure, stilling chamber pressure, and tunnel mass flow rate. The basic assumption of the flow calibration is that thermodynamic equilibrium exists in the tunnel stilling chamber and the gas becomes frozen in its vibrational mode at the nozzle sonic area. With the measured nozzle discharge coefficient, p_o, m, and A^*, and the use of real-gas nitrogen thermodynamic properties, inferred values of T_o are calculated. The gas is assumed to behave as a perfect gas downstream of the throat, and perfect-gas relationships are employed to arrive at free-stream flow properties. Measurements using local and total calorimeters, mass-flux probes, and nozzle wall static pressure measurements have confirmed the validity of the flow calibration procedures. Measured impact pressures are corrected for errors induced by probe viscous effects and the influence of energy flux into the probe orifice common to pressure measurements in heated low-density, hypersonic flows (Ref. 2).

Both the Mach 18 contoured nozzle and the 14-deg half-angle conical expansion nozzle were utilized to obtain direct comparative data on the influence of flow nonuniformity. For this reason, the flow condition was established in the conical nozzle to match, as closely as possible, the similarity parameters and wall conditions of the contoured nozzle. The models were tested at two axial locations in the conical nozzle flow field and one in the contoured nozzle. Since streamwise flow gradients are present in the conical nozzle, but not in the contoured nozzle, this produced three distinct flow conditions.

Figures 2a through e indicate pertinent flow field conditions. Unless otherwise stated, all free-stream conditions are those at the location of the model nose, with its position being either at the nozzle exit plane or 12 in. (30.5 cm) downstream of the exit plane. Free-stream conditions are tabulated in Tables Ia and b of the Appendix. The conditions shown in Figs. 2a through e and tabulated in Table I are nominal values with slight variations being present during a given tunnel run. An impact pressure probe was located at the model nose at a radial distance sufficient to ensure no shock interaction. Thus, run-to-run free-stream variations were accounted for in the data reduction process. The similarity parameter $M_\infty/(Re_\infty/in.)^{1/2}$ shown in Fig. 2d was an important criteria in selecting the flow conditions. Although exact duplication of unit similarity was not achieved, overlap between the contoured and conical nozzles resulted since the models were instrumented over a fairly long

surface length. Figures 2a through e illustrate the relative magnitude of conical flow effects on free-stream properties in the 14-deg nozzle. A 12-in. model located with its leading edge at the nozzle exit would be influenced by variations in free-stream properties as large as 25 percent. It should be noted that a 12-in. model would be an extreme size for this particular facility with model size less than one or two inches being normal. It should also be noted that the majority of other ground facilities which simulate high altitude and low unit Reynolds number flow utilize conical nozzles.

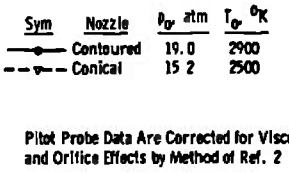

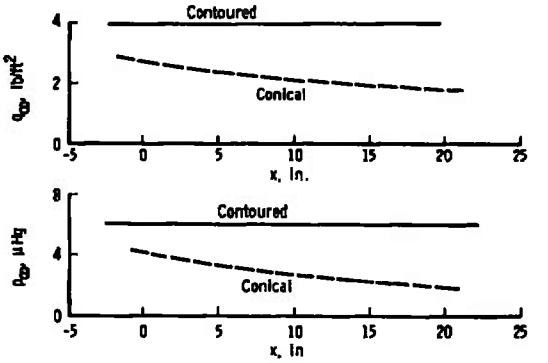

b. Free-stream Static and Dynamic Pressure

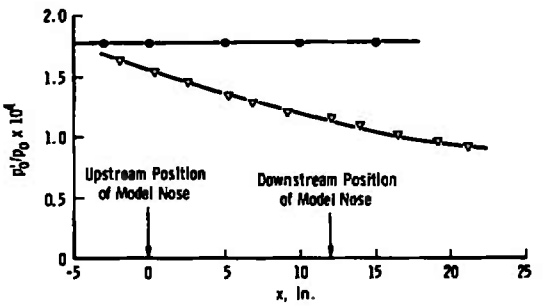

a. Pitot Pressure

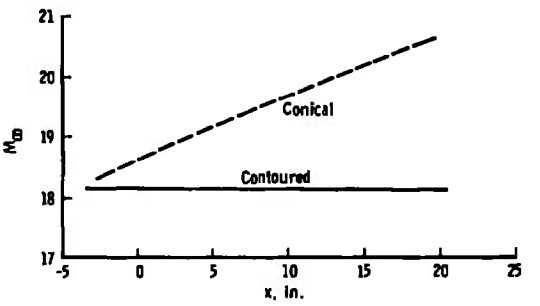

c. Mach Number

Fig. 2 Tunnel Test Section Flow Conditions

An estimate of the effect of source flow on heat-transfer measurements in Tunnel M is included in the present discussion. Source flow corrections require knowledge of facility nozzle dimensions, model length, instrumentation location and, for angle of attack data, point of rotation. It is also necessary to define the free-stream location relative to model position at which flow conditions are calculated. Normally, little of this information is available. Thus, it is usually impossible to determine to what degree source flow effects influenced a particular set of data from other facilities when reviewing the literature.

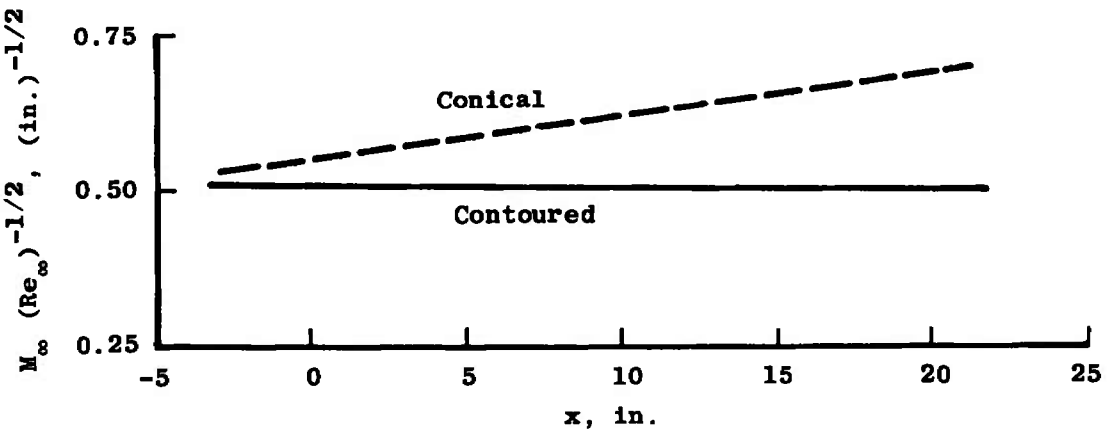

d. Similarity Parameter

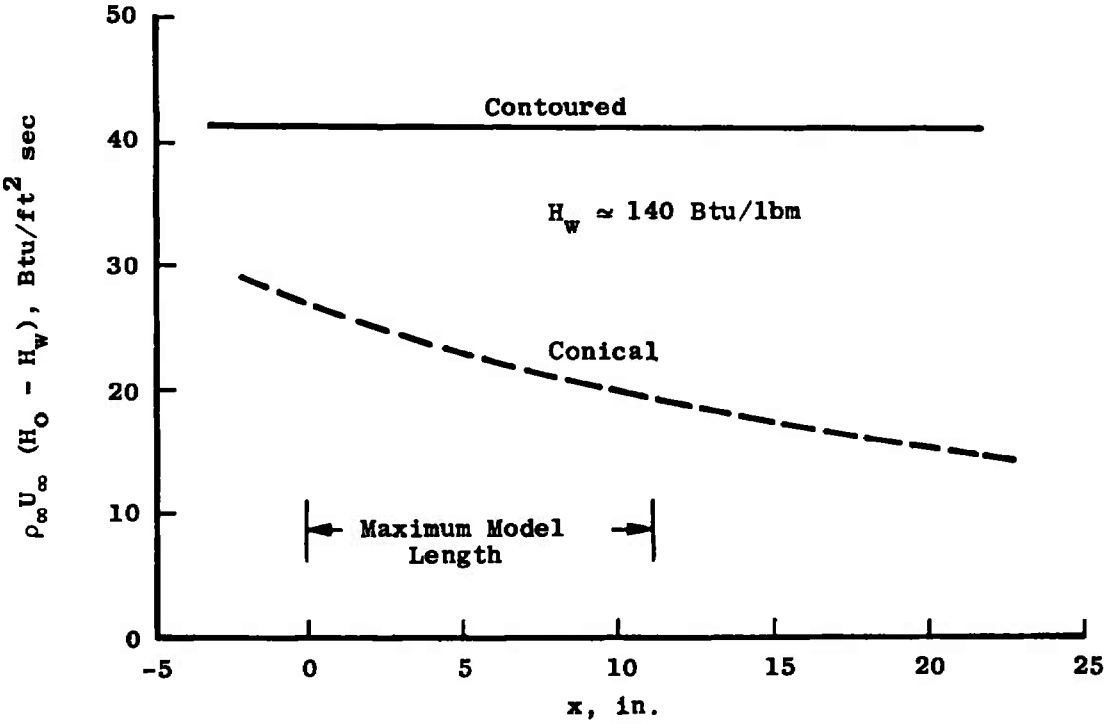

e. Energy Term

Fig. 2 Concluded

2.3 MODELS

A family of sharp and blunt 10-deg half-angle cones was designed and fabricated. With the exception of one spare nosepiece fabricated from stainless steel, all components were machined from brass. The

nose sections were not water cooled. All other components were water cooled from the back side by cooling coils. Figures 3a and b are photographs of the model components and one assembled configuration.

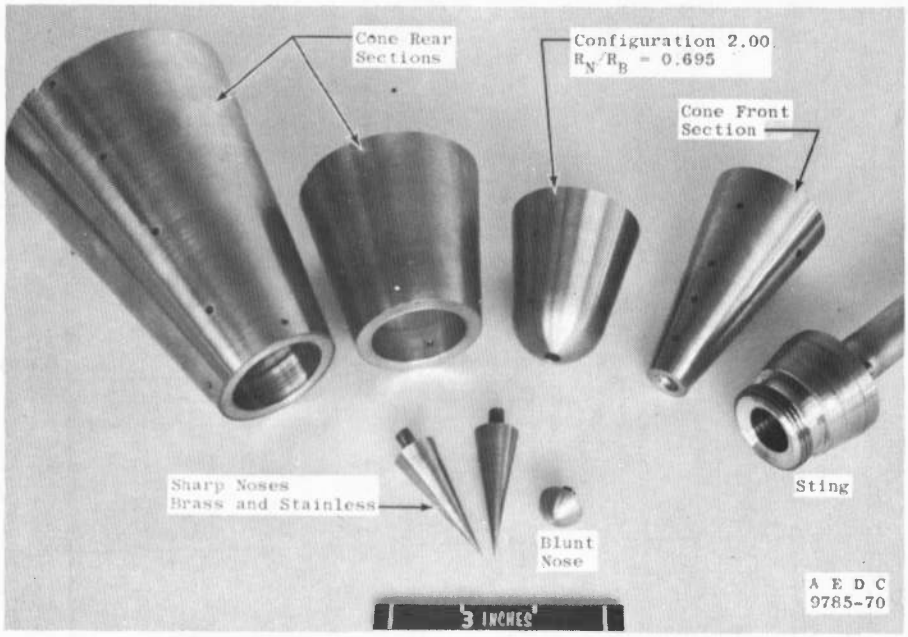

a. Components

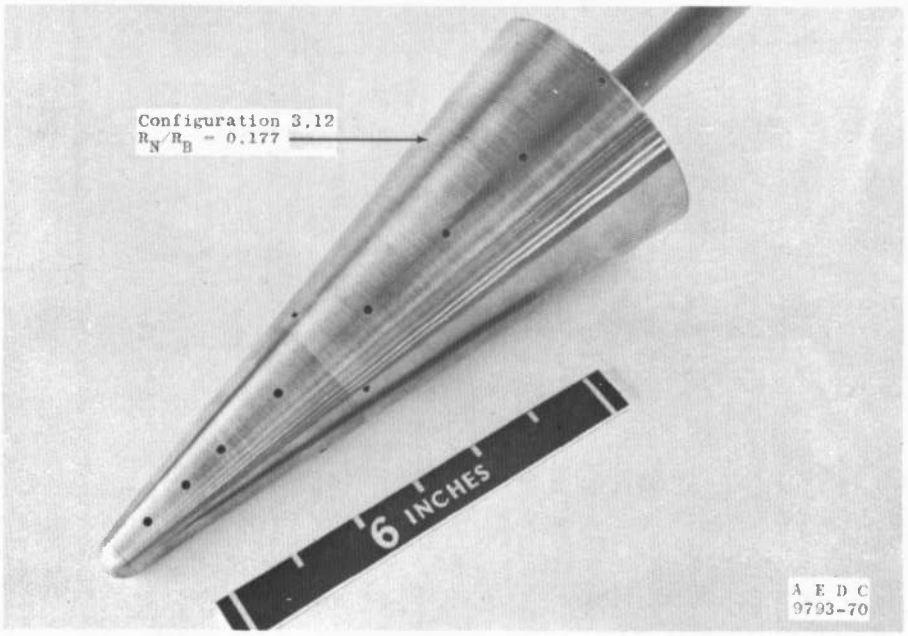

b. Assembled Model

Fig. 3 Model Photographs

Figure 4 is a sketch including the configuration code and model instrumentation locations. One axial model location was provided with four instrumentation ports located at intervals of 90 deg to study circumferential surface heating at angle of attack and monitor model alignment. The models were designed to accept steady-state Gardon-type heat-transfer gages which are described in Section 2.5. At the conclusion of the heat-transfer entry, the gages were removed and pressure tubes installed in their place. Results of the pressure investigation will be reported in a separate report.

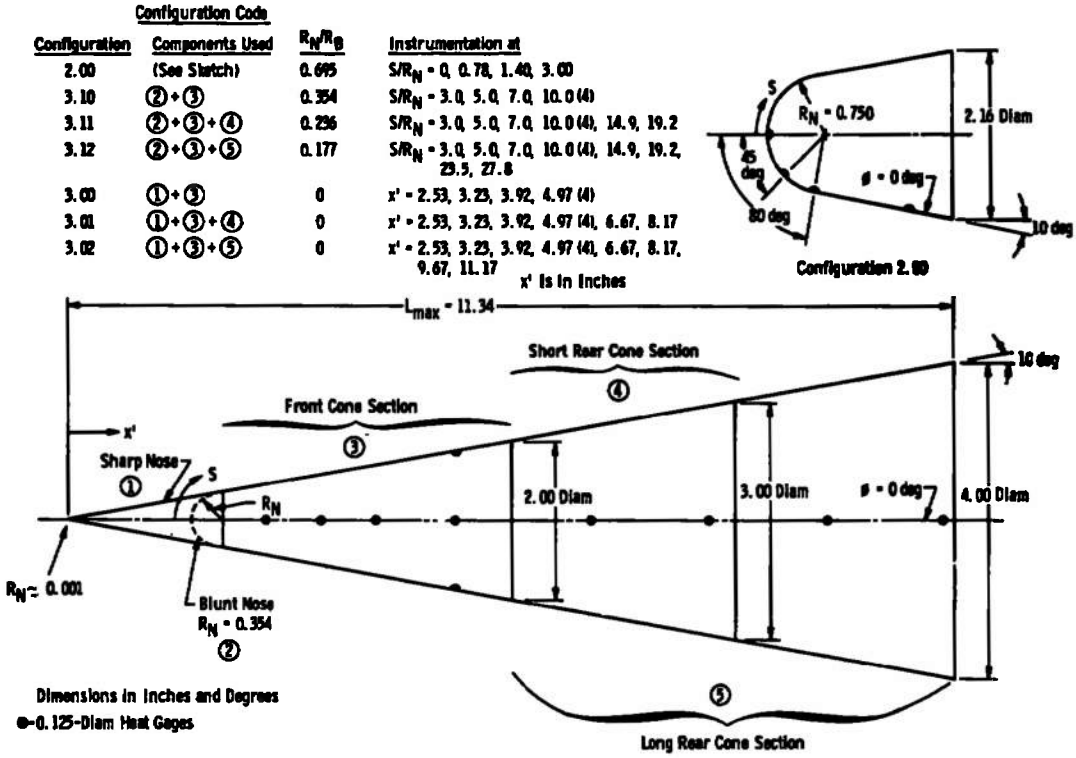

Fig. 4 Model Schematic and Configuration Code

2.4 TUNNEL INSTRUMENTATION AND DATA ACQUISITION SYSTEM

In addition to instrumentation necessary to monitor the arc heater and stilling chamber conditions, the following instrumentation is available in Tunnel M.

1. A low pressure level (3- to 30-mm Hg full-scale) primary standard pressure transducer system located within the tunnel test chamber.
2. Thermocouple system using Chromel®-Alumel® thermocouples for surface temperature measurements.
3. A one-component external axial force balance for measuring forces up to 0.2 lbf on aerodynamic bodies.
4. A two-component external normal-force and pitching-moment balance.
5. Steady-state Gardon heat-transfer gages and phase-change paint techniques are used for heat-transfer-rate measurements. The Gardon system was utilized in the present investigation and is described in some detail in Section 2.5.
6. Flow field and shock structure measurements can be made with an electron beam apparatus to obtain local values of temperatures, density, and velocity.

Model location and angle of attack are varied by remotely controlled drive mechanisms and monitored by linear potentiometers.

Data are recorded on the VKF Beckman 210 high-speed analog-to-digital acquisition system which scans all channels in about 1 sec and records data on paper tape. The raw data are then input into the VKF CDC-1604 B computer for data reduction. Data are also plotted on-line by mechanical plotters for quick analysis.

2.5 MODEL INSTRUMENTATION

A transducer which derives its basic principle of operation from the Gardon-type gage (Ref. 3), but has an order of magnitude greater sensitivity to incident heat flux has been developed at the AEDC for use in continuous wind tunnels. A photograph of a typical transducer is shown in Fig. 5. Transducer assemblies are installed in the wall of a model for heat flux measurements. Material considerations limit the maximum service temperature of the transducer to less than 350°F. Transducers whose nominal dimensions are 0.125-in. outside diameter by 0.25-in. length were used in these experiments. Aerodynamic wind tunnel heat flux data are obtained with the use of the following expression:

$$\dot{q} = C_1 E_o \tag{1}$$

The constant, C_1, is the transducer calibration factor and is determined experimentally. In aerodynamic testing, the parameter of interest is the convective heat-transfer coefficient, h, which is given by the expression:

$$h = \dot{q}/(T_G - T_w) \tag{2}$$

A transducer may be effectively utilized for aerodynamic heat flux measurements only if an accurate heat-transfer coefficient can be calculated from the test data. As shown by Eq. (2), a determination of the heat-transfer coefficient is dependent upon a knowledge of the transducer temperature. Since a temperature gradient exists across the sensing surface of the circular foil transducer, the temperature of the sensing surface is not clearly defined. However, the errors in the calculated heat-transfer coefficient are insignificant if the variation in T_w is small relative to the difference between the gas temperature, T_G, and the transducer sensing surface temperature. The high-sensitivity transducer provides an output signal of sufficient magnitude for obtaining accurate heat flux data with small variations in sensing surface temperature.

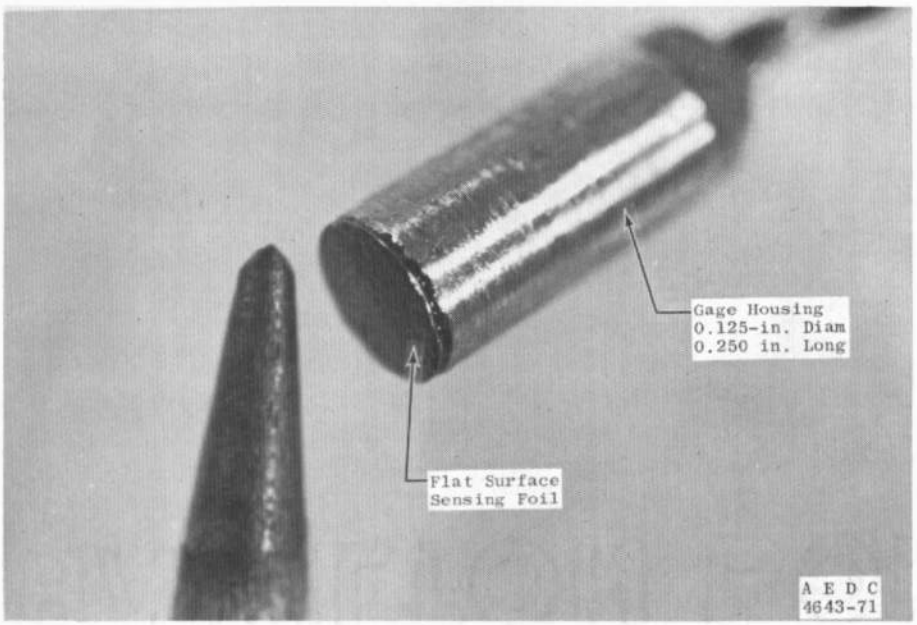

Fig. 5 Photograph of the High Sensitivity Heat-Transfer-Rate Transducer

Experimental calibration of the high-sensitivity transducer is accomplished with a radiant heat source. Calibration is achieved by exposing one or more transducers and heat flux standards to the same incident heat flux and measuring the output from each simultaneously. This procedure is repeated at different heat flux levels. Heat flux measurement standards are slug calorimeters which are designed and manufactured at the AEDC. All transducer calibrations are traceable to slug calorimeter standards. Transfer standards used with the radiant heat flux calibration apparatus are conventional Gardon-type transducers. In addition to calibration against slug calorimeter standards, calibrations were also performed on three transfer standard Gardon-type transducers at two independent calibration facilities. Calibration agreement was within 4 percent for the three transfer standards checked.

2.6 DATA PRECISION

Data precision is a function of many parameters. Based on calibration data, the accuracy of the model heat flux measurements is estimated to be within ±5 percent and repeatability and linearity within ±3 percent. Flow properties and Stanton number precision are estimated as follows:

Parameter	Absolute Accuracy	Percent
p_o, atm	±0.10	±0.5
T_o, °K	±120	±4.0
$p_{\acute{o}}$, μHg	±100	±2.0
M_∞	±0.26	±1.5
Re_∞, in.$^{-1}$	±100	±7.5
p_∞, μHg	±0.60	±10.0
$\rho_\infty U_\infty$, lbm/ft^2 sec	±1.6 x 10^{-5}	±7.5
$\dot{q}$, Btu/ft^2 sec	±0.05	±5.0
S_t	±0.012	±12.5
Angle of Attack, deg	±0.1	---

SECTION III
RESULTS AND DISCUSSION

3.1 PROCEDURE

As part of the study of the effect of nonuniform flow in the conical nozzle, data at angle of attack were obtained. The normal procedure was to initiate flow with the model at zero angle of attack and record all surface heat-transfer rates. An impact pressure probe measurement, located at the model nose station but at a radial distance sufficiently removed from the model to ensure no interference, was also recorded. Model angle of attack was then varied by rotating the model about a center of rotation midway between the model nose and base in small increments in the range $-9 \leq \alpha \leq 10$ deg with data being recorded at several positions. A final point was normally obtained with the model again near zero angle of attack. Machine plots were generated during the data reduction process to allow a rapid analysis of data quality to be made. Figure 6 indicates typical plots of Stanton number variation with angle of attack at constant free-stream flow conditions and selected model surface locations. Plots similar to these were machine generated for all model surface heat-transfer channels during each tunnel run. A typical run would require from one to two minutes after flow was established. All data reported herein were read from the fairing of curves such as those shown in Fig. 6. As can be seen, this procedure resulted in both windward and leeward* data being obtained. Since the absolute value of the heat flux decreased significantly in the latter case, data accuracy, repeatability, and scatter became worse as compared to the windward data at high angle-of-attack values.

3.2 STAGNATION POINT MEASUREMENTS

Configuration 2.00 (Fig. 4) was instrumented with a stagnation point gage, and measurements were made at all three flow conditions of the present investigation. Stagnation point data are tabulated in

*Actually, all of the data were windward since the angle-of-attack range was deliberately constrained to values less than the cone half-angle. However, the terms "most windward" and "least windward" are awkward, and it is common practice to use windward and leeward in their place.

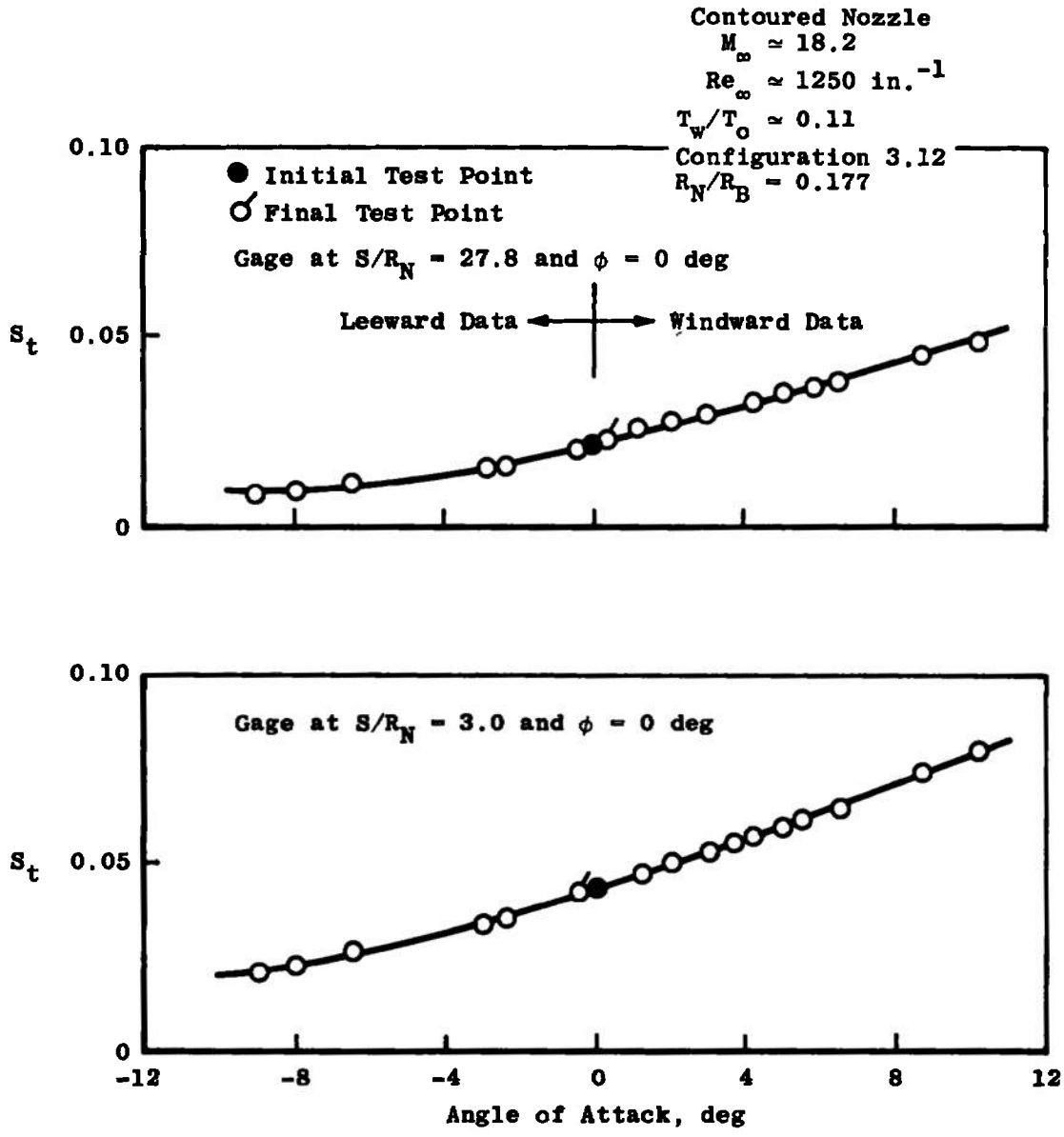

Fig. 6 Typical Blunt Cone Surface Heat-Transfer-Rate Variation with Angle of Attack

Table II and shown in Fig. 7. Comparisons are made to previous stagnation point heating rate measurements on a hemisphere-cylinder configuration (Ref. 4) and to the theoretical thin-shock solution of Cheng (Ref. 5). An adjustment to Cheng's results to account for the differences in density ratio using the method of Potter (Ref. 6) is also shown in Fig. 7. This adjusted curve was then used to infer stagnation point

heating rates to normalize blunt cone surface measurements presented later for cones of different nose radii. Agreement between the present 10-deg cone data and the hemisphere-cylinder data of Ref. 4 can be seen.

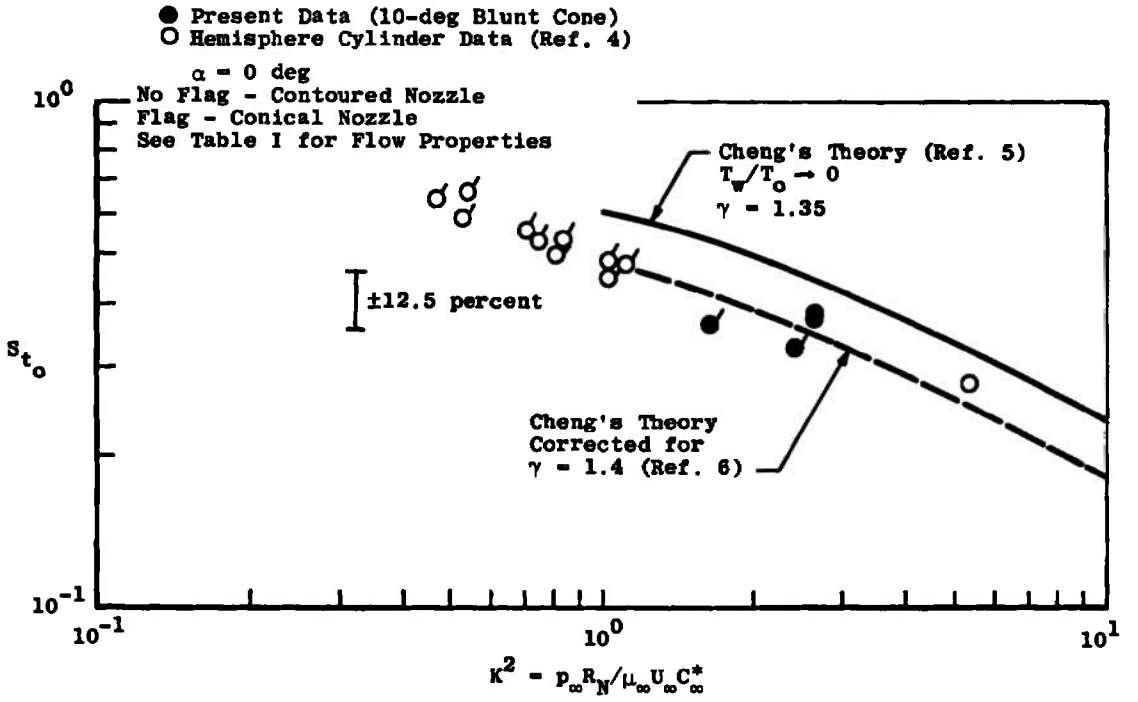

Fig. 7 Stagnation Point Heat-Transfer Rate on Configuration 2.00

It should be noted that values of S_{t_o} measured in the present study do not agree with Fay-Riddell theory which is appropriate for the higher Reynolds number flow regime with no wall or shock slip but would not be appropriate for the present conditions. The estimated precision of ±12.5 percent for this measurement is shown graphically on the data correlation. A more detailed discussion on rarefied flow effects on heat-transfer rate to spherical stagnation points is included in Ref. 6.

3.3 BLUNT CONE SURFACE HEATING RATES

Using stagnation point values inferred from Fig. 7, cone surface heat-transfer rates measured for the different configurations and flow

conditions were normalized and are shown in Fig. 8 as a function of cone surface location. Typical Stanton number data at α = 0 are tabulated in Table IIIa.

The data in Fig. 8a, obtained in the contoured nozzle, are compared to the laminar heat-transfer distribution theory of Lees (Ref. 7). An inviscid pressure distribution was used in the calculation shown in Fig. 8a. Experimental wall pressures were subsequently used but gave very little difference in calculated local wall heat-transfer rates.

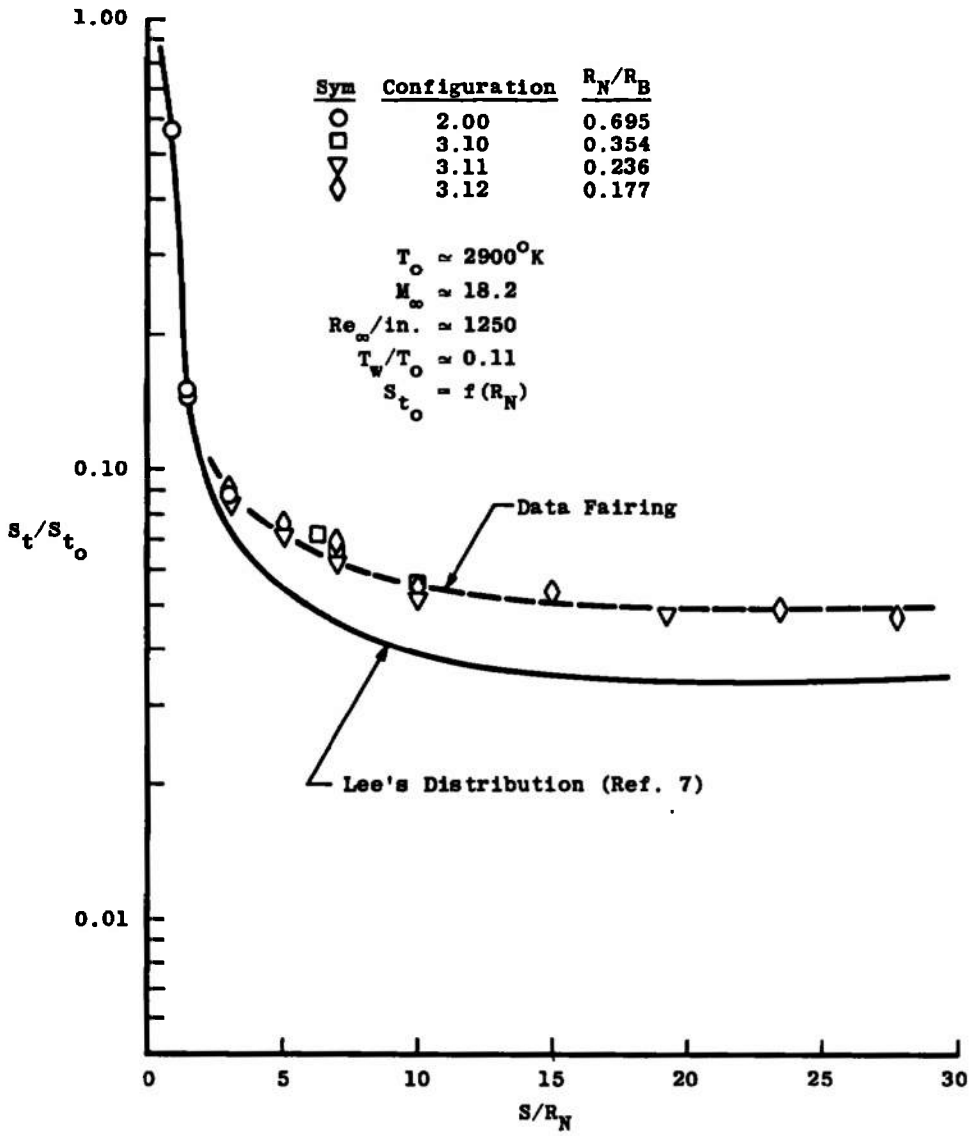

a. Contoured Nozzle

Fig. 8 Blunt 10-deg Cone Surface Heat-Transfer-Rate Distribution at α = 0 deg

The experimental value falls considerably above the theoretical solution. Results of a VKF computer code (Ref. 8), which allows calculation of blunt cone heat-transfer-rate distributions in uniform and source flow, are shown in Fig. 8b compared to data obtained in the conical nozzle. The difference between the two analytic results shown in this figure is an indication of the magnitude of the source flow effect on a blunt cone at zero angle of attack. The data from the conical nozzle, which should be compared to the solid line in Fig. 8b, also indicate a greater local heat-transfer rate than the analytic solution would predict.

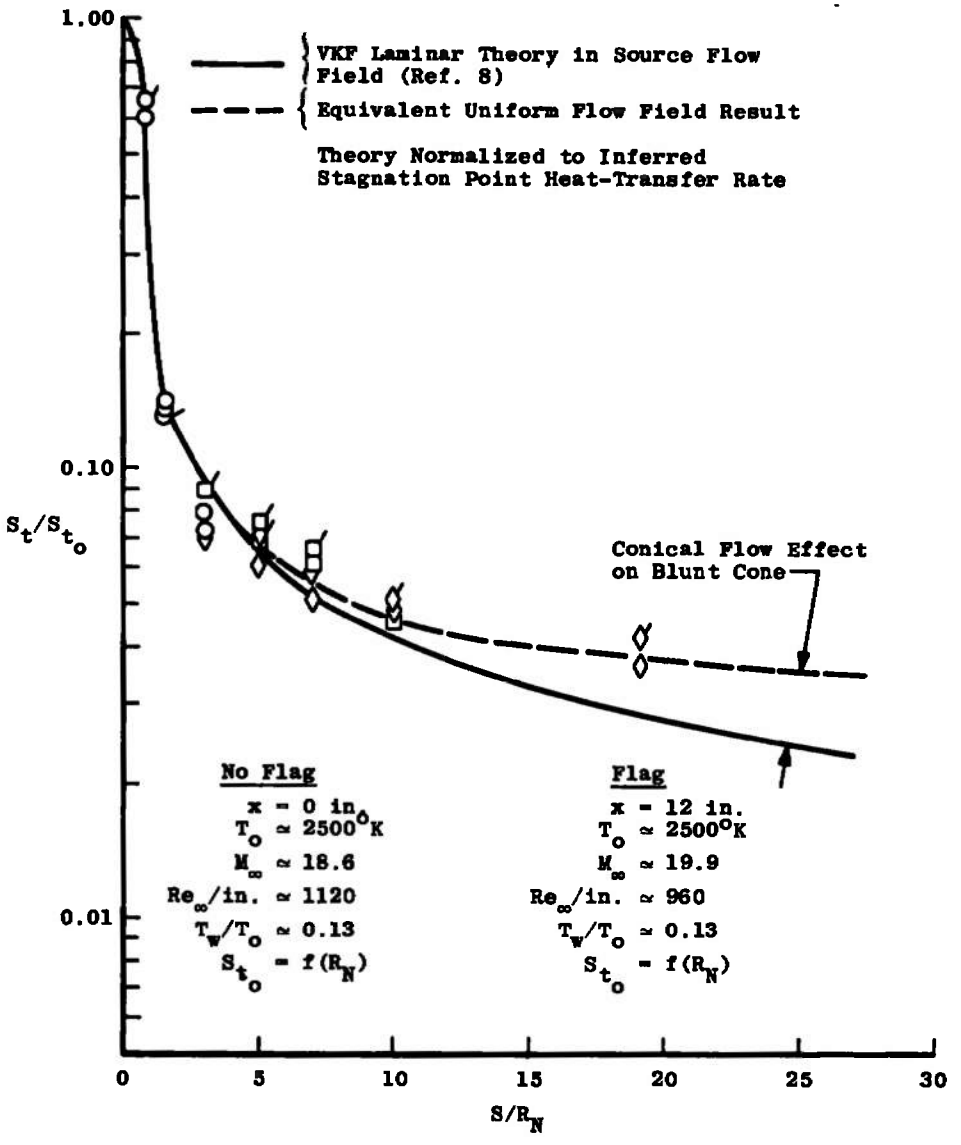

b. Conical Nozzle

Fig. 8 Concluded

An alternate method of presenting blunt slender cone Stanton numbers with laminar boundary layers and hypersonic free-stream conditions was proposed by Cheng (Ref. 9). He suggested that the parameter

$$S_t\,(\epsilon k)^{1/4}/\theta_c{}^2\bar{V}_*$$

when plotted as a function of

$$\theta_c{}^2\,x'/(\epsilon k)^{1/2}\,d$$

would account for the downstream influence of a slightly blunt leading edge as well as the displacement effect of the boundary layer. His analysis did not consider transverse curvature and boundary layer/shock layer merging. The viscous interaction similarity parameter $\bar{V}_*$ is defined in this case as

$$\bar{V}_* = M_\infty (C^*_\infty / Re_{\infty,d})^{1/2} \tag{3}$$

where

$$C^*_\infty = (\mu_*/\mu_\infty)\,(T_\infty/T_*) \tag{4}$$

and T_* is defined for blunt cones by Cheng (Ref. 9) as

$$T_* = (T_o/6)\left[1 + 3\,T_w/T_o\right] \tag{5}$$

The data are shown using these parameters in Fig. 9. Comparisons between the present data and those of Griffith and Lewis (Ref. 10), Horstman (Ref. 11), and Vas (Ref. 12) are also included. Although the present data are in good agreement with earlier measurements for similar cone angles (Ref. 10 and 12), there is a marked difference with the results of Horstman (Ref. 10) which pertain to 3-deg half-angle cones in low-temperature helium. This anomaly was discussed by Horstman, who postulated that Cheng's inviscid pressure distribution approximation is not valid for slender cones. Griffith and Lewis (Ref. 10) also discussed this problem and noted that Cheng's parameter is only valid at large Mach number and cone angles. They suggested a modification

of Cheng's parameter to allow correlation of very slender cones. However, since the present data were obtained at high free-stream Mach numbers and a fairly large cone angle, Cheng's original parameter was utilized. It does not appear that the modified form of Cheng's parameter suggested by Griffith would correlate the very slender cone data of Horstman with the present results. Data for the bluntest configuration (2.00) are omitted from Fig. 9 because the physical model violates Cheng's criteria for validity of the theory.

The effect of source flow can be seen in Fig. 9. Although both sets of data from the contoured and conical nozzles fall within the data spread of previous investigations, the data from the conical nozzle fall slightly below the contoured nozzle results.

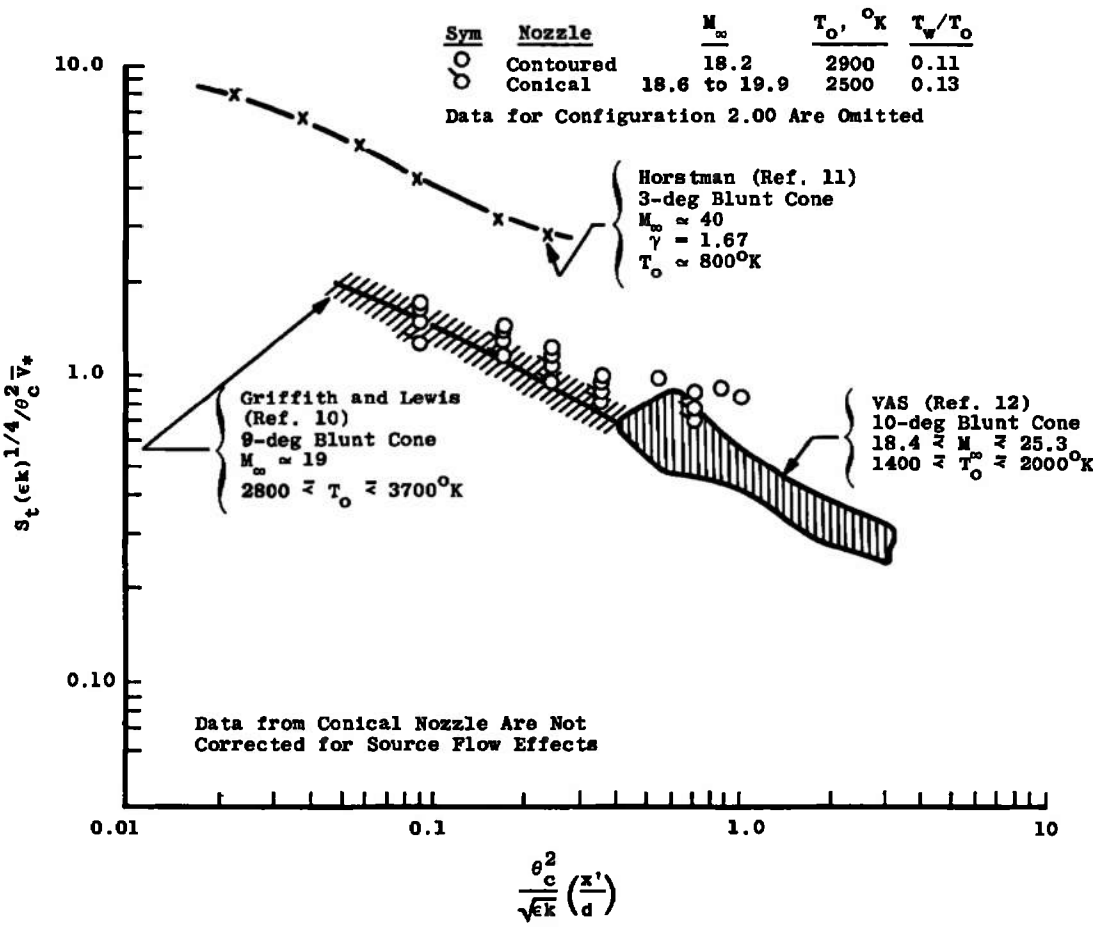

Fig. 9 Blunt Cone Surface Heat-Transfer-Rate Data Using Cheng's Parameters, α = 0 deg

A brief summary of blunt cone data obtained in the contoured nozzle at angle of attack is shown in Fig. 10. The longitudinal distribution is quite similar to the zero angle-of-attack data for both windward and leeward surfaces. Large circumferential effects are shown in Fig. 10b. No boundary-layer separation or cross flow effects could be detected from these data. Intermediate points between intervals of 90 deg were obtained by rolling the model and making repeat runs. The increase in heat transfer at $S/R_N \gtrsim 15$ for $\alpha = 10$ deg, observed by Horstman (Ref. 11) on a 3-deg blunt cone was not observed on the present 10-deg cone models. A complete tabulation of data at all flow conditions at angles of attack of 0, 5, 10, -5, and -9 deg is given in Table III.

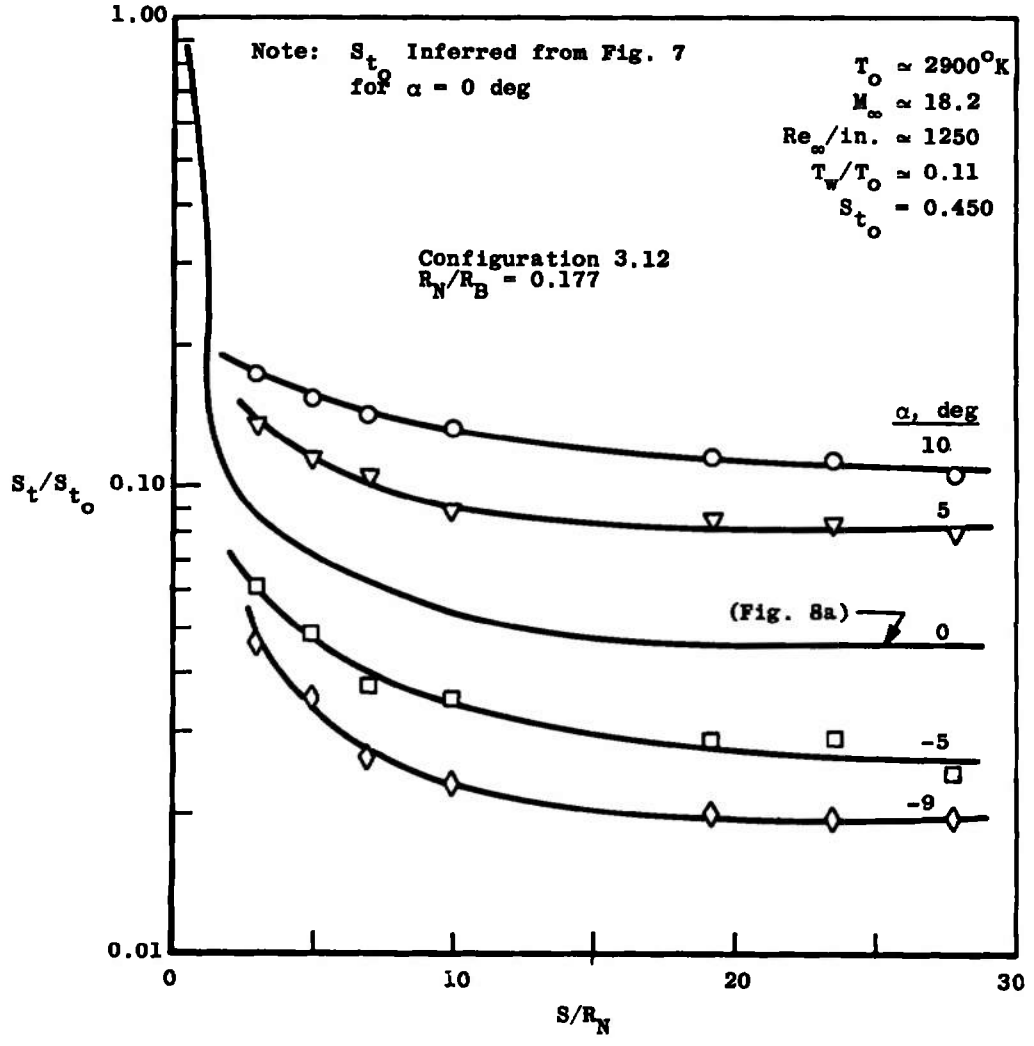

a. Longitudinal Distribution in the Contoured Nozzle

Fig. 10 Blunt Cone Data at Angle of Attack

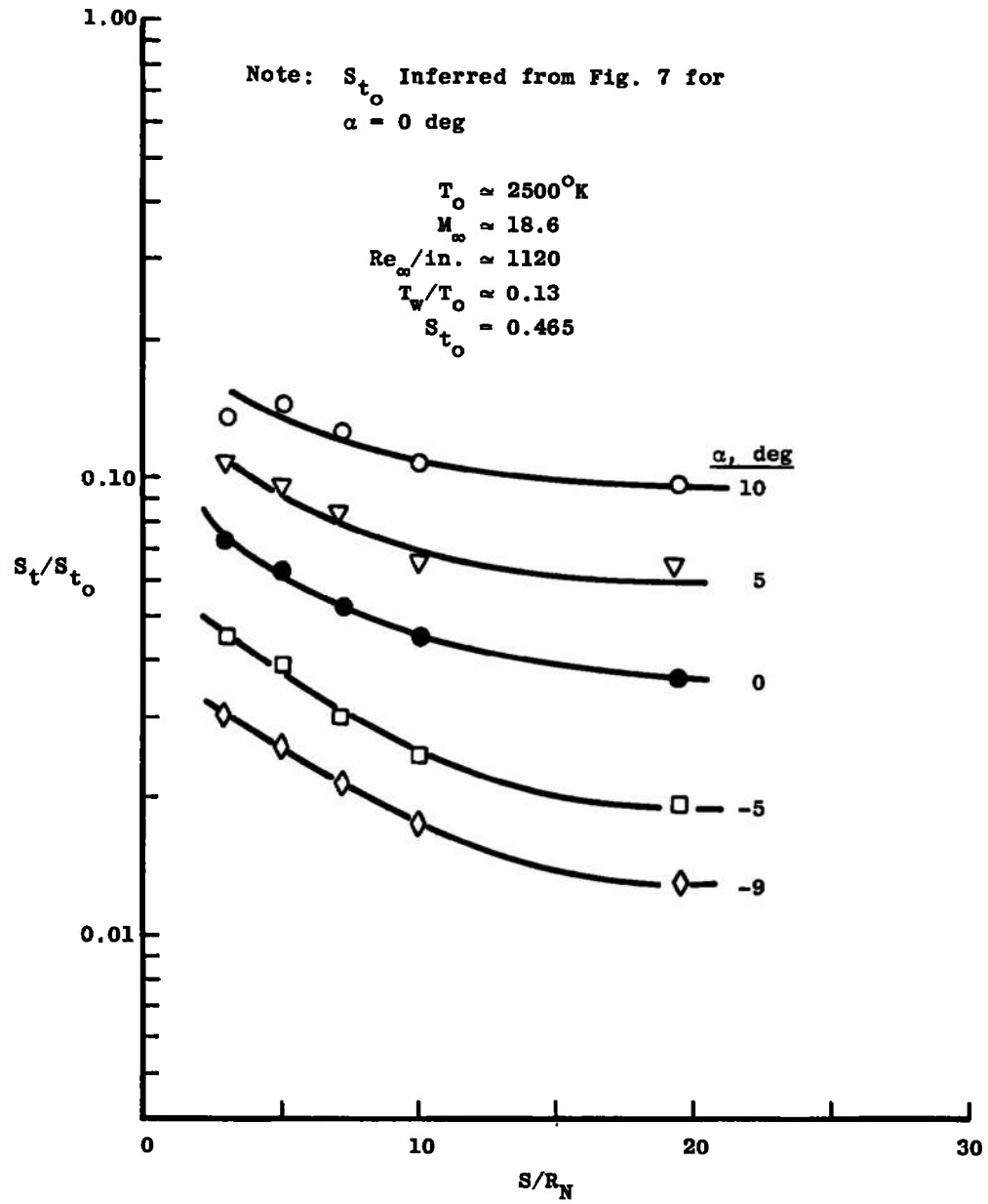

b. Longitudinal Distribution in the Conical Nozzle with Model Nose at x = 0 in.
Fig. 10 Continued

To the author's knowledge, there is no theoretical technique for correcting lee-side heat-transfer data for source flow effects at angle of attack. Windward ray data can be corrected, although utilization of complex computer codes is necessary. Since the present zero angle-

of-attack data indicate a maximum source flow effect of about 25 percent, no detailed correction of the windward ray angle-of-attack data was attempted. Also, since the parameter $\bar{V}_*$ defined in Eq. (3) was nearly constant between the two separate nozzles used, a cross plot of data such as shown in Figs. 10a and b would indicate the magnitude of the source flow error. In the range tested, $-9 \leq \alpha \leq 10$ deg, the difference is about 20 to 25 percent for windward ray data but increases to about 40 percent for the leeward ray data. These figures would apply only to configuration 3.12 because model length influences source flow effects.

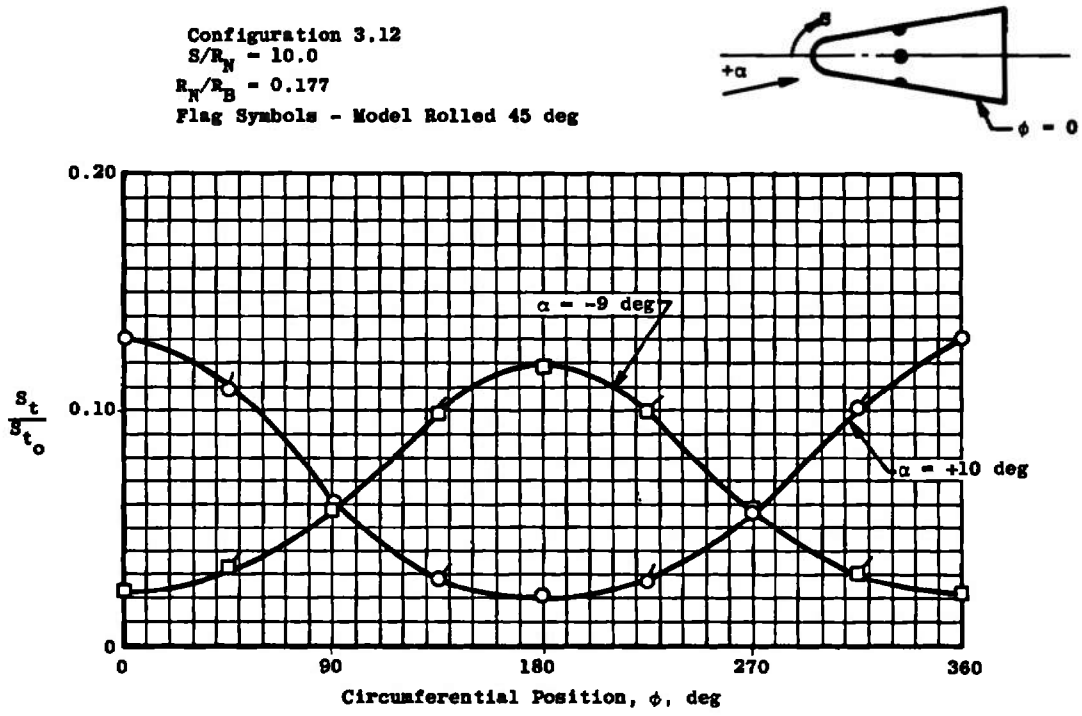

c. Circumferential Distribution in the Contoured Nozzle
Fig. 10 Concluded

3.4 SHARP CONE SURFACE HEATING RATES

The number of experimental and theoretical studies of laminar heat transfer to sharp cones is large, and no effort is made herein to review all of the studies available in the open literature.

A correlation technique suggested by Cheng (Ref. 13) and a technique based on the reference enthalpy approach extended to an "effective" cone approach are used in the present analysis. More rigorous theoretical models, which include the effect of surface velocity slip and temperature jump, shock-boundary-layer merging, and transverse curvature are becoming common in the literature. The work of Rubin et al., Shorenstein, and Maus (Refs. 14 through 16) are three of the more recent studies. A first order theory computer code supplied by Adams (Ref. 17) is used to develop a correlation parameter based on the reference enthalpy approach.

Surface data obtained on sharp leading-edge configurations in highly viscous hypersonic flow regimes are sometimes presented using the parameter

$$\bar{V}_* = M_\infty (C^*_\infty / Re_{\infty,x'})^{1/2} \tag{6}$$

where, from Eq. (4),

$$C^*_\infty = (\mu_*/\mu_\infty)\,(T_\infty/T_*)$$

T_* is defined by Cheng (Ref. 13) for sharp cones as

$$T_*/T_o = T_w/T_o + 1/2\,(1 - T_w/T_o) - 1/3\,\cos^2\theta_c \tag{7}$$

The differences between Eqs. (3) and (6) and Eqs. (5) and (7) should be noted. Although the numerical differences in $(C^*_\infty)^{1/2}$ calculated using Eqs. (5) and (7) are small, the effect on the absolute value of $\bar{V}_*$ brought about by using the diameter in Eq. (3) as opposed to axial length in Eq. (6) is quite large.

The present sharp cone, zero angle-of-attack Stanton number data using $\bar{V}_*$ as defined in Eq. (6) for correlation purposes are shown in Fig. 11 and tabulated in Table IVa. Figure 11a contains the data from the contoured nozzle, while 11b presents conical flow results. A summary plot is shown in Fig. 11c. The laminar theory of Adams (Ref. 17) is shown on these data plots. While comparison is excellent for the conical nozzle, this is believed to be fortuitous since the theoretical model was not designed for the merged flow regime where

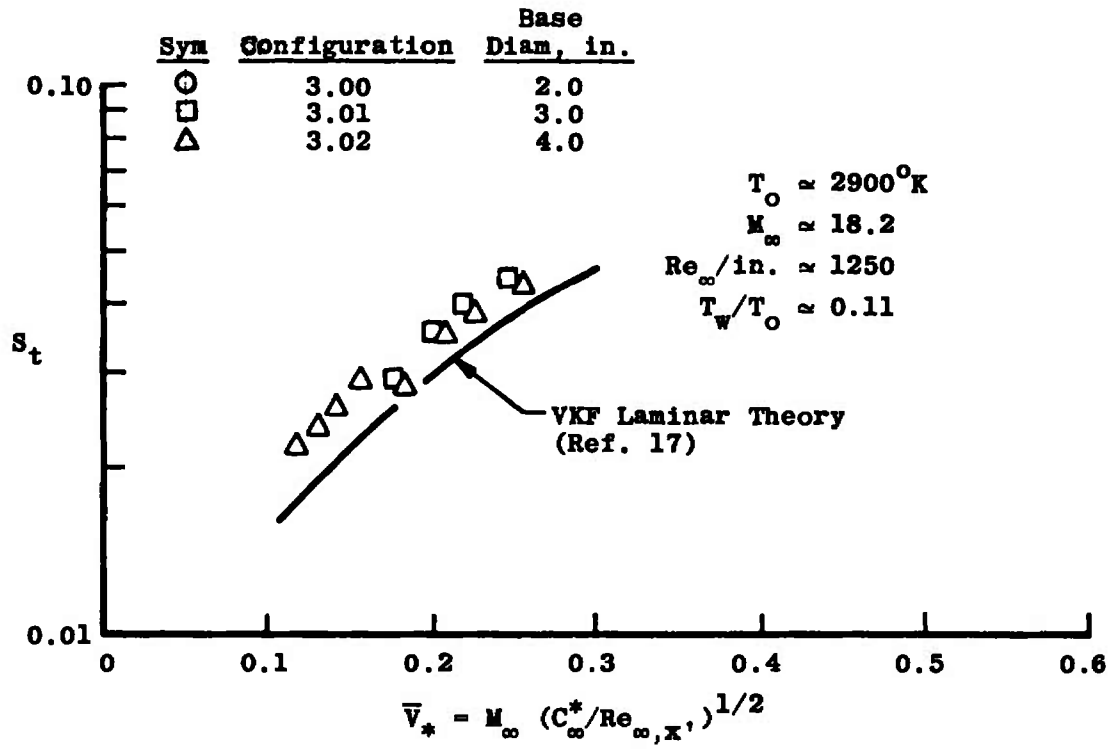

a Contoured Nozzle

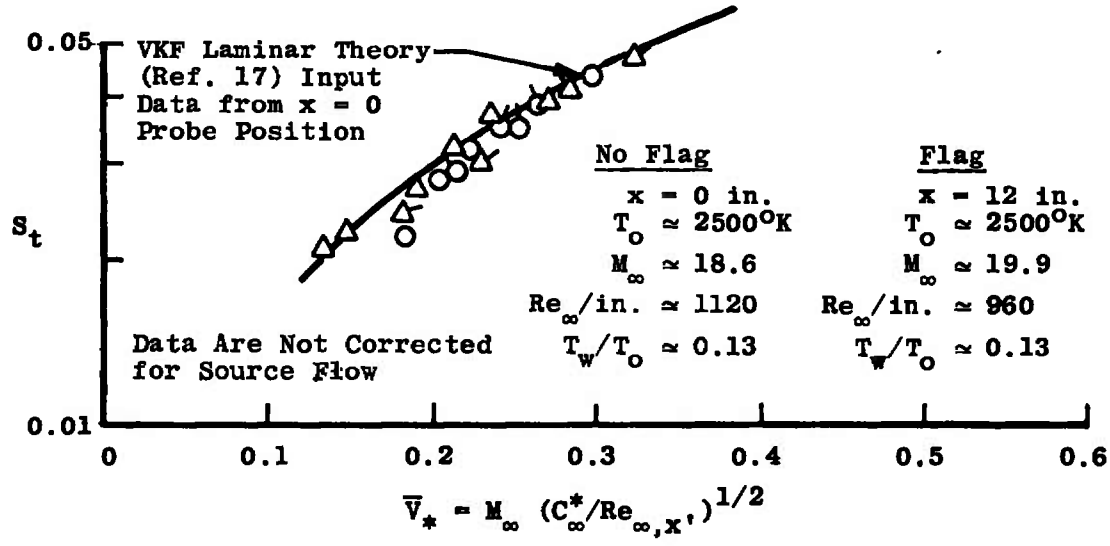

b. Conical Nozzle

Fig. 11 Sharp 10-deg Cone Surface Heat-Transfer-Rate Distribution at α = 0 deg

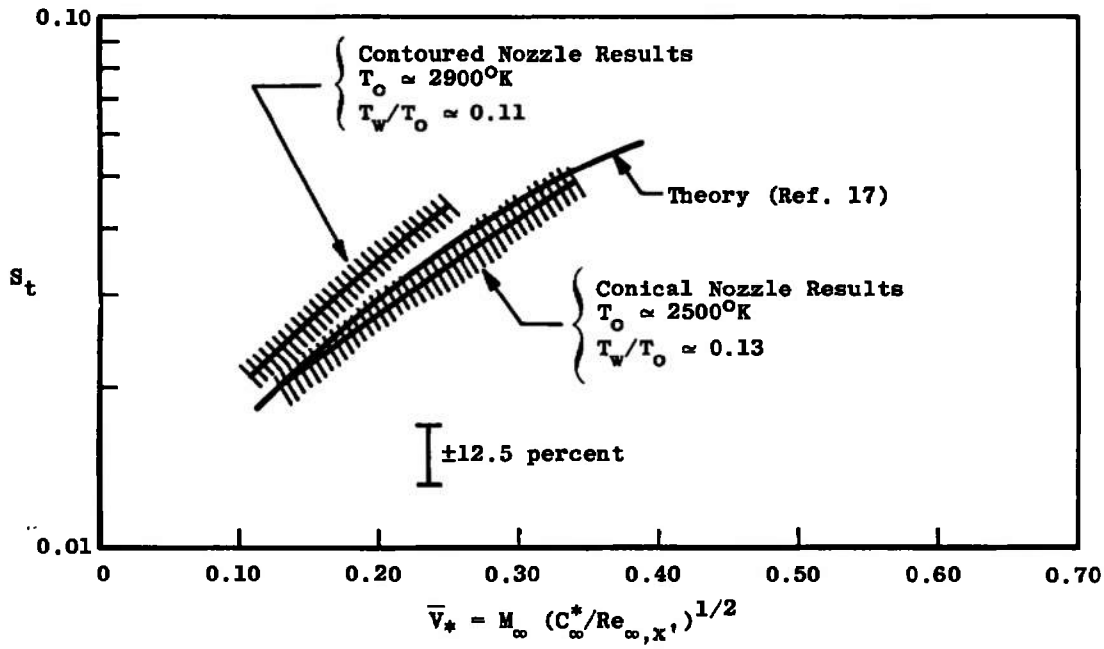

c. Summary Plot
Fig. 11 Concluded

transverse curvature and slip effects might influence the measurements. Also, the theory is a perfect gas solution while the data were obtained in a facility which produces some degree of nonequilibrium. The effect of this can be quite noticeable in heat-transfer studies because the theoretical approach calculates a perfect gas stagnation enthalpy based on free-stream conditions which is greater than actual stilling chamber conditions.

Since similitude was, for all practical purposes, exact between the two sets of data shown in Fig. 11, the difference in absolute value of Stanton number shown in Fig. 11c is probably due only to source flow effects on one group of the data. A higher order Newtonian approach has been developed in the VKF to correct surface heat transfer on sharp cone models located in a strong source flow field. For data in which flow conditions are defined at the nose of the model, the resulting expression for an equivalent uniform flow Stanton number is

$$\bar{S}_t = S_t \left[\frac{\left(p_e/p_\infty \left\{ I_\infty(\gamma, \xi) + (p_e/p_\infty - 1) \left[1/(1+\xi)\right]^3 \right\} \right)^{1/2}}{\left(\left[1/(1+\xi)\right]^{2\gamma} + \left[p_e/p_\infty - 1\right] \left[1/(1+\xi)\right]^4 \right)} \right] \tag{8}$$

where the uncorrected Stanton number S_t is defined using measured model heat flux and free-stream properties at the model nose and the pressure ratio p_e/p_∞ is for a uniform flow field. The geometric parameter ξ is defined as the axial distance from the model nose to a given instrumentation location divided by the axial distance from the nozzle apparent source to the model nose.

The source flow integral $I_\infty(\gamma, \xi)$ is developed as

$$I_\infty(\gamma, \xi) = (3/\xi^3) \int_0^\xi \frac{\xi^2 \, d\xi}{(1 + \xi)^{2\gamma}} \tag{9}$$

which approaches unity as ξ approaches zero.

An examination of Eq. (8) reveals that source flow effects on heat transfer are dependent on nozzle length, cone length, cone angle, instrumentation location on the cone surface, and free-stream Mach number. As the pressure ratio p_e/p_∞ becomes large, Eq. (8) quickly approaches the limit

$$\overline{S_t} = S_t \Big/ \left[1/(1 - \xi)\right]^{5/2}; \quad p_e/p_\infty \longrightarrow \infty \tag{8a}$$

The applicability of using Eq. (8a) rather than Eqs. (8) and (9) must be determined on an individual basis. For the flow conditions, model size, and conical nozzle length of the present investigation, the latter equation was found to be suitable.

It is sometimes reported that a "correction" for source flow errors on a particular model was accomplished by calculating the free-stream gradients along the length of the model and inputting local values in the tunnel data reduction program. This does not constitute a complete correction for three-dimensional models in a radial source flow field.

As was noted in Section 2.2, an extremely large model was employed in the present investigation to magnify source flow errors which resulted in the geometric parameter ξ having a maximum value of 0.182. Investigations reported in the literature present data obtained on models with ξ as large as 0.5 or 0.7. These studies often ignore this possible source of data error. For a given value of ξ,

source flow correction decreases with decreasing cone angle. However, for fixed model diameter, decreasing cone angle results in longer models and increasing values of ξ.

The data from the longest model (configuration 3.02) were hand corrected for source flow effects using the procedure outlined above and the results are shown in Fig. 12. Although the correction appears somewhat low at the forward end of the model and slightly large at the aft end, agreement between the contoured and conical nozzle data is improved when the correction is accomplished. The theoretical correction varied from 9 to 50 percent for these data. A correction of about 15 to 25 percent would have resulted in very good agreement with the contoured nozzle results.

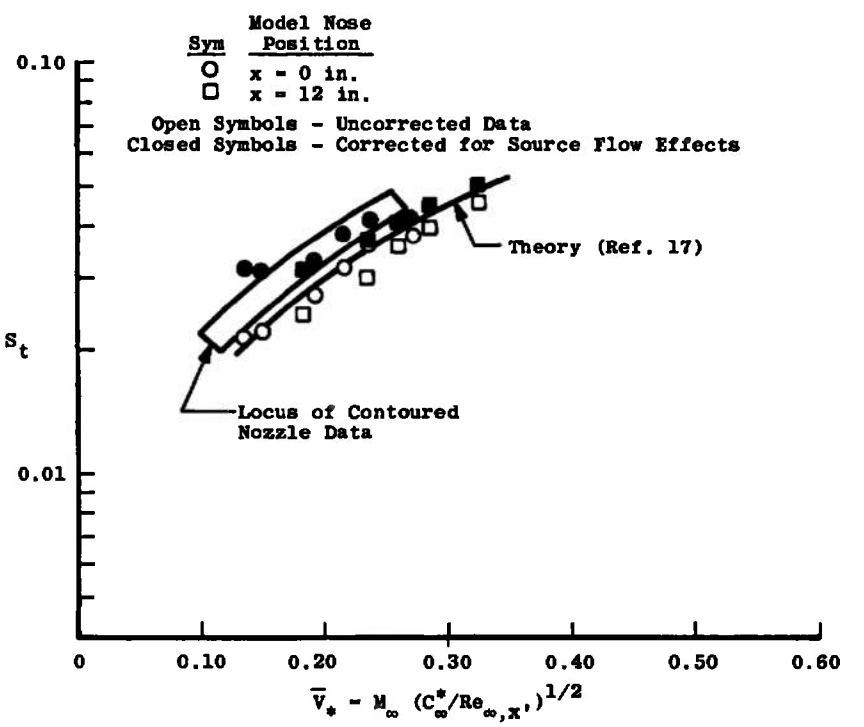

Fig. 12 Correction for Source Flow Effects for Configuration 3.02

Numerous correlation techniques are available for zero angle-of-attack laminar sharp cone heat-transfer data. A common method (Ref. 18) is to present the data based on Cheng's (Ref. 13) parameter as

$$\frac{S_t}{\sin \theta_c} (1 - T_w/T_o) = f\left(\frac{1}{\bar{V}_*^2 \gamma \cos \theta_c}\right) \tag{10}$$

Waldron (Ref. 18) pointed out that this method is not independent of cone angle basing this statement on data from 5-, 6.3-, 9.0-, 10.0-, and 20.0-deg cones. In particular, departure from the viscous layer analysis of Cheng (Ref. 13) is dependent on cone angle since transverse curvature effects increase as cone angle decreases. A collection of 10-deg cone data is shown in Fig. 13 using this method. Data from the conical nozzle shown in Fig. 13 are not corrected for source flow effects and are slightly lower than the contoured nozzle data. Allowing for this correction, the present data would tend to indicate a slightly higher level than the data of Ref. 18 and would be in good agreement with the data of Kienappel* (Ref. 19) and Vas (Ref. 12). Higher order leading-edge theories of Rubin (Ref. 14) and Maus (Ref. 15) are also indicated in Fig. 13. Both approaches indicate a slightly higher value of heat-transfer rate than the experiments indicate.

An additional correlation of zero angle-of-attack data based on a reference enthalpy approach was developed. The method, which is an empirical approach to account for the effects of compressibility, is useful in that it related quantities for a compressible flow to those of an incompressible flow. The method should remove the effect of cone angle in the flow regime where transverse curvature and other higher order effects are not strong.

The correlation requires the data to be plotted in the form

$$S_{t_{e,aw}}/(C_e^*)^{1/2} = K' (Re_{e,\ell}) \tag{11}$$

where C_e^* is defined as

$$C_e^* = (\mu_*/\mu_e) (T_e/T_*) \tag{12}$$

*These data were obtained in the DFVLR facility at Gottingen, Germany, as part of the current cooperative program.

and T_* is redefined as the temperature corresponding to the Eckert reference enthalpy

$$H_* = 0.5(H_w + H_e) + 0.22\sqrt{Pr}\ U_e^2/2 \qquad (13)$$

The subscript e refers to inviscid conditions at the outer edge of the cone boundary layer, and values were obtained from tables of inviscid cone properties published by Jones (Ref. 20). The local Stanton number $S_{t_{e,aw}}$ is calculated using local inviscid boundary-layer edge conditions and the adiabatic wall enthalpy rather than total enthalpy. A laminar recovery factor of 0.843 was used in the correlation with Prandtl number being assumed at 0.71.

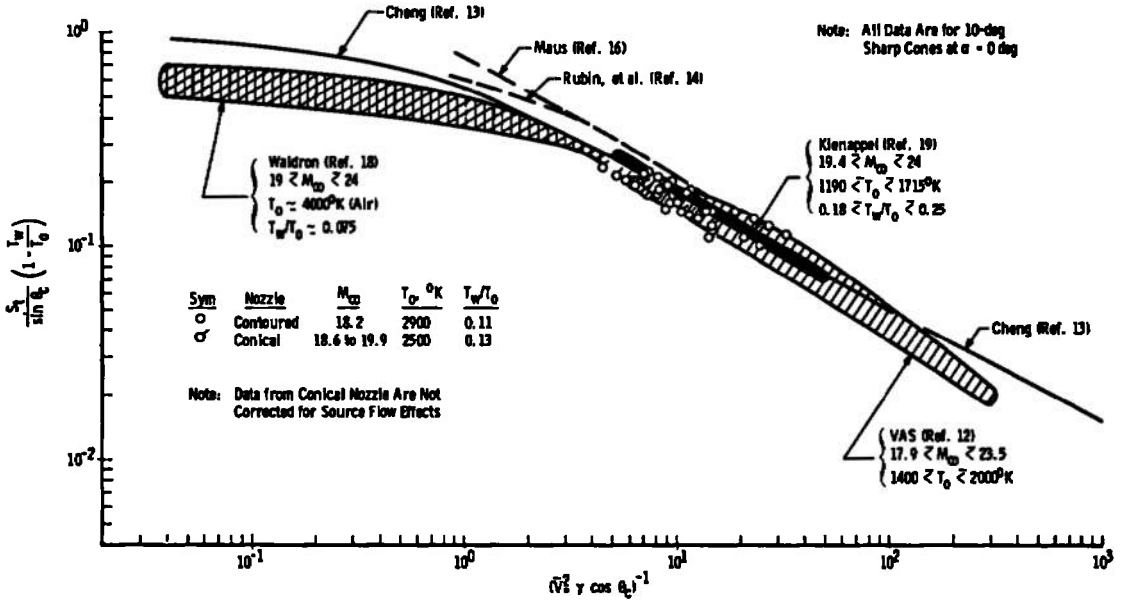

Fig. 13 Sharp Cone Surface Heat-Transfer-Rate Data Using Cheng's Parameters, α = 0 deg

In order to check the validity of the correlation technique, theoretical solutions using various input conditions were obtained using a computer code supplied by Adams (Ref. 17). The results are shown in Fig. 14. Input conditions vary over a wide range of wall temperature, cone angle, free-stream Mach number, and unit Reynolds numbers and include conditions corresponding to typical reentry flight values. Correlation is excellent over the entire range studied but

could be expected to fail when local edge Mach numbers become low. Values of this parameter are shown for each solution obtained.

The inclusion of the constant of proportionality between viscosity and temperature (C_e^*) is often omitted in correlations of experimental results. The confusing manner in which various theoretical approaches define this constant and the reference temperature used tempts one to neglect it altogether. In fact, this often results in little error since the numerical value of $(C_e^*)^{1/2}$ or $(C_\infty^*)^{1/2}$ varies only slightly and is near unity for ground facility data. However, if flight data are being compared to ground facility data, the inclusion of this parameter is necessary. The correlation of theoretical solutions shown in Fig. 14 would be unsatisfactory without the reference temperature viscosity term.

One of the approximate analysis techniques in common usage to estimate windward ray heating rates on slender cones at incidence is the so-called "effective cone" approach in which a zero angle-of-attack calculation is performed on an "effective cone" which has a cone half-angle equal to the physical cone half-angle plus the physical cone angle

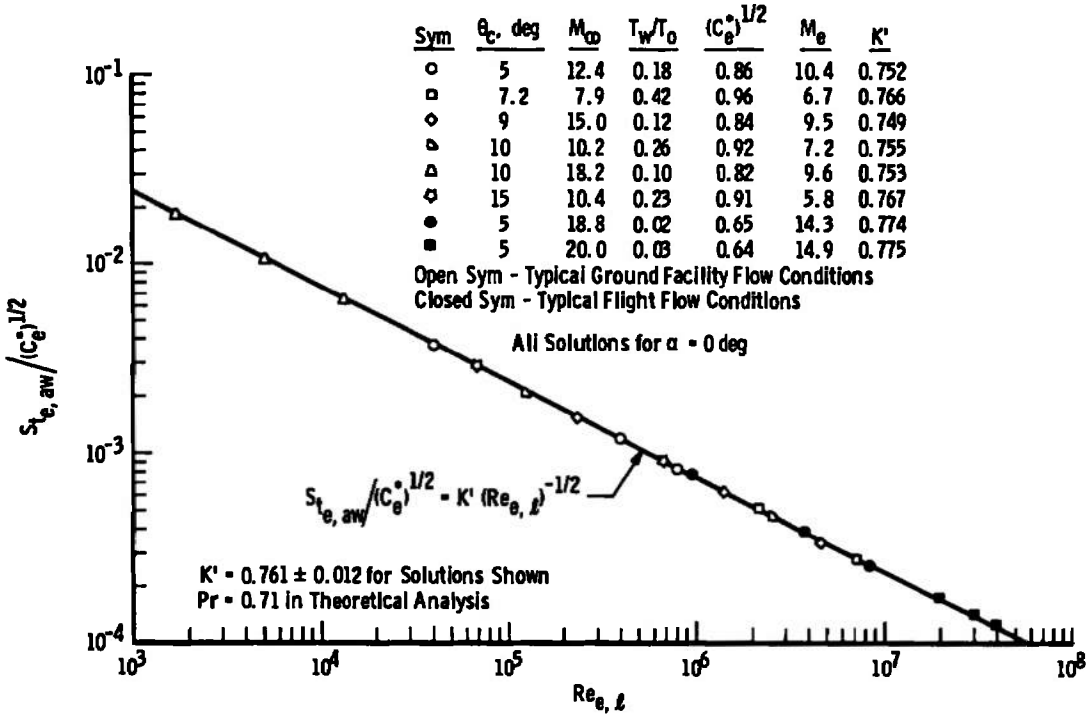

Fig. 14 Correlation of Laminar Sharp Cone Heat-Transfer Theory of Adams (Ref. 17)

of attack. The effect of crossflow on the windward ray boundary-layer structure is neglected using this procedure. Since the correlation shown in Fig. 14 is valid for a wide range of cone angles, it is in effect such an "effective cone" analysis. Windward ray data obtained at 5-deg angle of attack on a 10-deg sharp cone could be expected to correlate with a 15-deg cone model tested at the same local flow conditions but at zero angle of attack if no crossflow effects were present. Unfortunately, such crossflow effects are quite often very strong for laminar boundary layers, and indiscriminate use of such a procedure to estimate windward ray heating rates can result in severe underprediction of heat transfer and skin friction. A discussion of this is given by Adams (Ref. 21).

The present results are shown correlated in Fig. 15, and the results suggest that crossflow is not important for the present model under these low-density flow conditions. The data from the contoured nozzle fall above the first order theory of Ref. 17 which, as pointed out earlier, is not surprising since transverse curvature, shock merging, wall slip, etc., were not included in the theoretical model. The data from the conical nozzle (Fig. 15b) are closer to the theory but are presumed to be too low due to source flow effects, as shown in Fig. 12. The weak interaction theory of Ref. 22 which includes transverse curvature effects agrees fairly well with the contoured nozzle results.

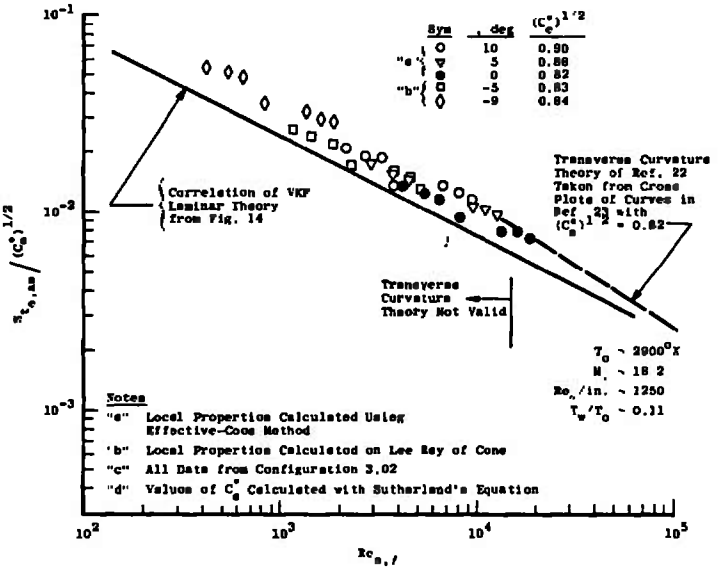

a. Contoured Nozzle

Fig. 15 Correlation of Present Sharp Cone Data in the Range $-9 \leq \alpha \leq 10$ deg

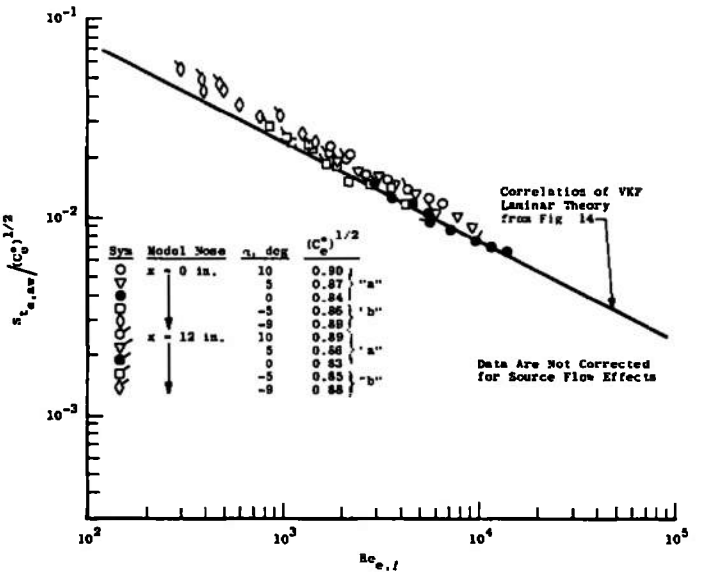

b. Conical Nozzle
Fig. 15 Concluded

The data shown in Fig. 15 at positive angle of attack (windward) were correlated using the "effective cone" approach. That is, local properties on the windward ray of a 10-deg cone at 10-deg angle of attack were assumed to be the same as on a 20-deg cone at zero angle of attack. However, the leeward data obtained at angles of attack of -5 and -9 deg required that local flow properties be calculated for the lee ray following the procedure of Ref. 20.

No correlation technique can be considered adequate until independent data are included. By combining the 10-deg sharp cone data of the present study with the more recent work of Berry, et al. (Ref. 23), a complete set of sharp cone, low-density heat-transfer data in the range $3 \leq \theta_c \leq 30$ deg can be correlated. The results are shown in Fig. 16. The Chapman Rubensin viscosity proportionality term C_e^* was calculated for the data of Ref. 23 using the power law $\mu \sim T^{\omega}$ where ω is a function of T^* for μ^* and T_e for μ_e. Values of T^* were calculated from Eq. (13) and perfect-gas nitrogen. Values of C_e^* for each data set are indicated in Fig. 16. Theoretical Blausis-Mangler and Probstein-Elliott transverse curvature results shown in Fig. 16 were taken directly from Ref. 23 and adjusted by the appropriate value of C_e^*. These previous experiments in conical nozzles are compared to the present conical and contoured nozzle data. Some interesting conclusions can be drawn from these results. First, both the

Blausis-Mangler and Adams theoretical solutions give good agreement with the entire set of data obtained in conical flow. The small-cone-angle data, which should be strongly influenced by transverse curvature, do not appear to reflect this influence. The data from the present contoured nozzle are above the trend of all of the conical nozzle results and they agree with the theoretical transverse curvature results for a 10-deg cone.

An exact analysis of the effect of source flow on the data of Ref. 23 is not possible with the information given. However, an estimate was made using Eq. (8) and the results indicated that the "estimated" maximum error of ten percent given in Ref. 23 is considerably low for the 3- and 5-deg angle cones, and these data should be shifted upward by a significant amount in Fig. 16. This, of course, would ruin the correlation over the entire range from $3 \leq \theta_c \leq 30$ deg shown, but the correlation of the low-cone-angle data may be fortuitous in the present case. The correction does not appear to be large enough to force agreement with the transverse curvature theory. However, it was pointed

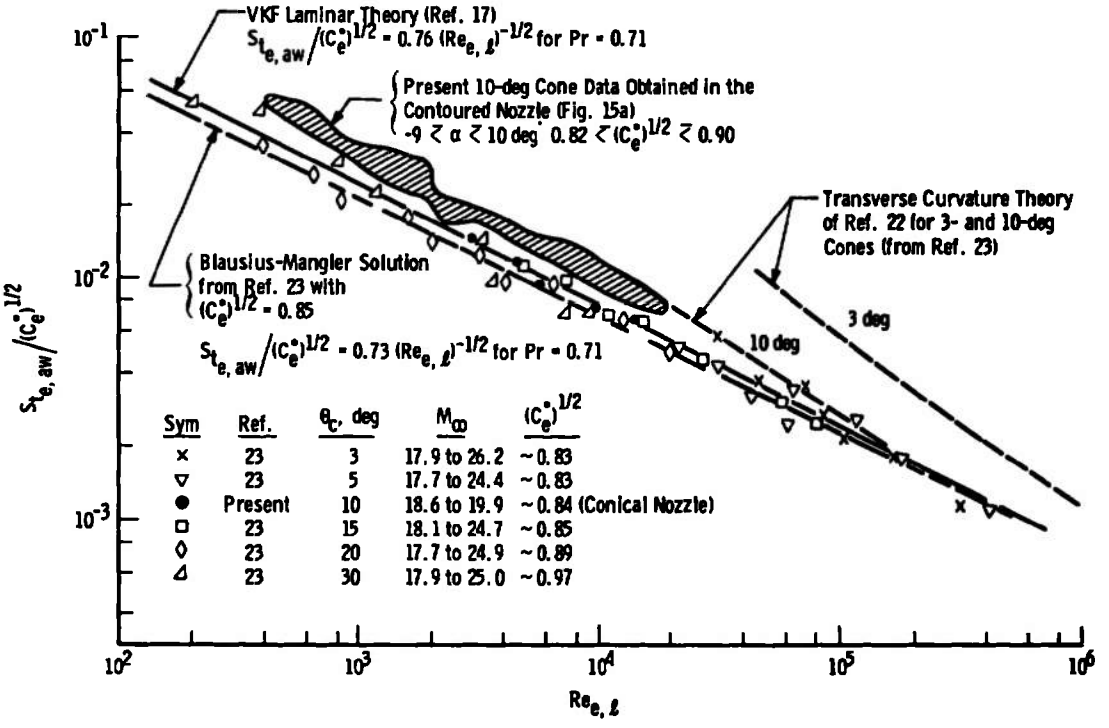

Fig. 16 Correlation of Previous Sharp Cone Data with Present Results

out in Ref. 23 that the theoretical results cannot be considered entirely valid at the flow conditions and model size used in that investigation. For the present Tunnel M zero angle-of-attack data, the limit of the validity of the transverse curvature theory would be at a lower value of $Re_{e,\ell}$ of about 1.5×10^4.

SECTION IV
CONCLUDING STATEMENT

The results of the present investigation can be summarized as follows:

1. Stagnation point measurements on blunt 10-deg cones are in good agreement with previous hemisphere measurements at the same free-stream flow conditions. Comparison with Cheng's thin shock layer theory is good if an adjustment is made for differences in density ratio between Cheng's formulation and the experimental conditions.
2. Correlation of the data from the blunt, slender cone model at zero incidence is in good agreement with previously published data.
3. Blunt 10-deg cone heat-transfer-rate distributions indicate local heating rates above thin boundary-layer theory at values of S/R_N greater than 3.0. Data obtained in both parallel and source flow on long slender blunt bodies indicate that errors can result due to source flow effects.
4. Data obtained at angle of attack indicated no significant crossflow or boundary-layer separation, but errors due to source flow effects appear to increase with angle of attack.
5. Data on sharp, slender cones at zero incidence are in good agreement with previously published data at similar flow conditions.
6. Correlation of sharp cone data was accomplished using a reference enthalpy approach extended to an "effective cone" angle correlation for windward ray data obtained at angle of attack.

7. Source flow effects at α = 0 deg were moderate with a maximum error of about 25 percent being observed at the aft end of the largest sharp model. The theoretical prediction of source flow errors utilized herein appears to over-estimate the correction necessary at the aft end of the model and under-estimate the effect at the forward end.

8. It is shown that source flow effects on heat-transfer-rate measurements are significant and care should be taken in facilities subject to such influences. The technology is available to design contoured nozzles producing uniform free-stream flows.

REFERENCES

1. Kinslow, M., Busby, M. R., and Potter, J. L. "Low-Density Boundary-Layer Modulation by Suction in a Hypersonic Nozzle." AEDC-TR-72-178 (AD754276), January 1973.

2. Kinslow, Max and Potter, J. Leith. "Reevaluation of Parameters Relative to the Orifice Effect." Paper Presented at the 7th International Symposium on Rarefied Gas Dynamics, Pisa, Italy, 1970. To be published by Academic Press.

3. Gardon, Robert. "An Instrument for the Direct Measurement of Intense Thermal Radiation." The Review of Scientific Instruments, Vol. 24, No. 5, May 1953.

4. Boylan, David E. "Laminar Convective Heat Transfer Rates on a Hemisphere Cylinder in Rarefied Hypersonic Flow." AIAA Journal, Vol. 9, No. 8, Aug 1971, pp. 1661-1663.

5. Cheng, H. K. "Hypersonic Shock-Layer Theory of the Stagnation Region at Low Reynolds Number." CAL Report No. AF-1285-A-7, Cornell Aeronautical Laboratory, Inc., Buffalo, New York, April 1961.

6. Potter, J. Leith. "The Transitional Rarefied-Flow Regime." Rarefied Gas Dynamics, Supp. 4, Vol. II, Academic Press, New York, 1967, pp. 881-937.

7. Lees, Lester. "Laminar Heat Transfer over Blunt-Nosed Bodies at Hypersonic Flight Speeds." Jet Propulsion, Vol. 26, No. 4, April 1956, pp. 259-269.

8. Mayne, A. W., Jr. and Dyer, D. F. "Comparison of Theory and Experiment for Turbulent Boundary Layers on Simple Shapes at Hypersonic Conditions." Proceedings of the 1970 Heat Transfer and Fluid Mechanics Institute, Stanford University Press, 1970, pp. 168-188.

9. Cheng, H. K. "Hypersonic Flow with Combined Leading-Edge Bluntness and Boundary-Layer Displacement Effect." CAL Report No. AF-1284-A-4, August 1960.

10. Griffith, B. J. and Lewis, Clark H. "Laminar Heat Transfer to Spherically Blunted Cones at Hypersonic Conditions." AIAA Journal, Vol. 2, No. 3, March 1964, pp. 438-444.

11. Horstman, C. C. "Blunt Slender Cones in Viscous Hypersonic Flow." AIAA Journal, Vol. 8, No. 10, October 1970, pp. 1853-1859.

12. Vas, I. E. "An Experimental Study of the Flow about a Slender Cone at Hypersonic Speeds." Ph. D. Dissertation, Department of Aeronautics and Astronautics, New York University, New York, May 1970.

13. Cheng, H. K. "The Blunt Body Problem in Hypersonic Flow at Low Reynolds Number." IAS Paper No. 63-92, presented at the IAS 31st Annual Meeting, New York, January 1963.

14. Rubin, S. G., Lin, T. C., Pierucci, M., and Rudman, S. "Hypersonic Interactions Near Sharp Leading Edges." AIAA Journal, Vol. 7, No. 9, September 1969, pp. 1744-1751.

15. Shorenstein, Michael L. "The Hypersonic Leading Edge Problem." II. Wedges and Cones, MIT Fluid Mechanics Laboratory Report, April 1971. Also see AIAA Journal, Vol. 10, No. 9, September 1972.

16. Maus, J. R. "An Analytical Investigation of Viscous Shock-Layer Flow Near the Leading Edge of Slender Bodies Under Low Density Hypersonic Conditions." AEDC-TR-73-102 (AD762505), June 1973.

17. Adams, John C., Jr. "Implicit Finite-Difference Analysis of Compressible Laminar, Transitional, and Turbulent Boundary Layers along the Windward Streamline of a Sharp Cone at Incidence." AEDC-TR-71-235 (AD734535), December 1971.

18. Waldron, H. F. "Viscous Hypersonic Flow over Pointed Cones at Low Reynolds Numbers." AIAA Journal, Vol. 5, No. 2, February 1967, pp. 208-217.

19. Kienappel, J. "Experimentelle Untersuchung Des Örtliches Wärmeüberganges an Schlanken Kegeln In Verdünnter Hyperschallströmung." Preliminary report of the DFVLR, April 1971.

20. Jones, D. J. "Numerical Solutions of the Flow Field for Conical Bodies in a Supersonic Stream." NRCC Aeronautical Report LR-507, July 1968.

21. Adams, John C., Jr. "Evaluation of Windward Streamline Effective Cone Boundary Layer Analyses." Journal of Spacecraft and Rockets, Vol. 9, No. 9, September 1972, pp. 718-720.

22. Probstein, R. F. and Elliott, E. "The Transverse Curvature Effect in Compressible Axially Symmetric Laminar-Boundary-Layer Flow." Journal of Aeronautical Sciences, Vol. 23, No. 3, March 1956.

23. Berry, Carl T., Vas, Irwin E., and Bogdonoff, Seymour M. "An Experimental Investigation of Laminar Heat Transfer to Cones at Hypersonic Speeds." ARL 72-0159, November 1972.

APPENDIX
TABLES

TABLE I
NOMINAL FLOW CONDITIONS
a. Customary Units

Gas - N_2

Nozzle	Contoured	Conical	Conical
Monitor Probe Location	---	Exit	x = 12 in.
p_o, atm	19.0	15.2	15.2
T_o, °K	2900	2500	2500
H_o, Btu/lbm	1500	1275	1275
M_∞	18.2	18.6	19.9
Re_∞, $in.^{-1}$	1250	1120	960
p_∞, μHg	6.00	4.20	2.60
T_∞, °K	45.0	35.0	33.0
U_∞, ft/sec	8165	7350	7575
ρ_∞, lbm/ft^3	3.73×10^{-6}	3.27×10^{-6}	2.22×10^{-6}
λ_∞, in.	0.022	0.022	0.031
q_∞, lb/ft^2	3.90	2.80	1.98
Re_2, $in.^{-1}$	45	41	28
S_∞	15.2	15.5	16.5
$p_{o'}/p_o$	1.767×10^{-4}	1.56×10^{-4}	1.13×10^{-4}

TABLE I (Concluded)
b. SI Units

Gas - N_2

Nozzle	Contoured	Conical	Conical
Monitor Probe Location	---	Exit	x = 12 in.
p_o, atm	19.0	15.2	15.2
T_o, °K	2900	2500	2500
H_o, J/gm	3489	2966	2966
M_∞	18.2	18.6	19.9
Re_∞, cm^{-1}	492	442	377
p_∞, N/m^2	0.80	0.56	0.347
T_∞, °K	45.0	35.0	33.0
U_∞, m/sec	2489	2240	2309
ρ_∞, kg/m^3	5.97×10^{-5}	5.24×10^{-5}	3.56×10^{-5}
λ_∞, cm	0.0559	0.0559	0.0787
q_∞, N/m^2	186.7	134.0	94.80
Re_2, cm^{-1}	17.72	16.14	11.02
S_∞	15.22	15.54	16.5
$p_{o'}/p_o$	1.767×10^{-4}	1.56×10^{-4}	1.13×10^{-4}

TABLE II
STAGNATION POINT HEAT-TRANSFER-RATE DATA

Configuration 2.00 (Fig. 4)

Nozzle	q_o, Btu/ft^2 sec	S_{t_o}	K^2
Contoured	14.5	0.37	2.56
Contoured	14.8	0.38	2.58
Conical (x = 0 in.)	8.0	0.33	2.45
Conical (x = 12 in.)	6.6	0.37	1.63

TABLE III
TABULATION OF BLUNT CONE STANTON NUMBERS
a. α = 0 deg, ϕ = 0 deg

Config.*	Flow Conditions**	S/R_N									
		0.784	1.40	3.00	5.00	7.00	10.0	14.9	19.2	23.5	27.8
2.00	Contoured	0.197	0.052	0.030	---	---	---	---	---	---	---
	Conical x = 0 in.	0.230	0.048	0.025	---	---	---	---	---	---	---
	Conical x = 12 in.	0.274	0.056	0.035	---	---	---	---	---	---	---
3.10	Contoured	---	---	0.040	0.032	0.030	0.025	---	---	---	---
	Conical x = 0 in.	---	---	0.039	0.033	0.028	0.022	---	---	---	---
	Conical x = 12 in.	---	---	0.048	0.040	0.034	0.026	---	---	---	---
3.11	Contoured	---	---	0.039	0.032	0.029	0.024	---	0.023	---	---
3.12	Contoured	---	---	0.043	0.035	0.031	0.025	0.025	0.023	0.023	0.022
	Conical x = 0	---	---	0.033	0.029	0.024	0.021	---	0.017	---	---
	Conical x = 12 in.	---	---	0.046	0.039	0.034	0.031	---	0.024	---	---

*Figure 4
**Table I

TABLE III (Continued)
b. α = 5 deg, ϕ = 0 deg

Config. *	Flow Conditions**	S/R_N									
		0.784	1.40	3.00	5.00	7.00	10.0	14.9	19.2	23.5	27.8
2.00	Contoured	---	---	0.043	---	---	---	---	---	---	---
	Conical x = 0 in.	0.251	0.065	0.043	---	---	---	---	---	---	---
	Conical x = 12 in.	0.302	0.076	0.048	---	---	---	---	---	---	---
3.10	Contoured	---	---	0.059	0.048	0.046	0.040	---	---	---	---
	Conical x = 0 in.	---	---	0.059	0.049	0.045	0.049	---	---	---	---
	Conical x = 12 in.	---	---	0.068	0.060	0.052	0.042	---	---	---	---
3.11	Contoured	---	---	0.054	0.047	0.044	0.037	---	0.038	---	---
3.12	Contoured	---	---	0.061	0.051	0.047	0.040	---	0.038	0.037	0.036
	Conical x = 0 in.	---	---	0.050	0.044	0.039	0.030	---	0.030	---	---
	Conical x = 12 in.	---	---	0.065	0.057	0.051	0.041	---	0.038	---	---

*Figure 4
**Table I

TABLE III (Continued)
c. α = 10 deg, ϕ = 0 deg

Config.*	Flow Conditions**	S/R_N									
		0.784	1.40	3.00	5.00	7.00	10.0	14.9	19.2	23.5	27.8
2.00	Contoured	---	---	0.055	---	---	---	---	---	---	---
	Conical x = 0 in.	0.282	0.088	0.060	---	---	---	---	---	---	---
	Conical x = 12 in.	0.330	0.097	0.067	---	---	---	---	---	---	---
3.10	Contoured	---	---	0.077	0.066	0.065	0.061	---	---	---	---
	Conical x = 0 in.	---	---	0.084	0.072	0.067	0.072	---	---	---	---
	Conical x = 12 in.	---	---	0.093	0.082	0.075	0.061	---	---	---	---
3.11	Contoured	---	---	0.074	0.067	0.064	0.057	---	0.056	---	---
3.12	Contoured	---	---	0.079	0.070	0.064	0.059	---	0.053	0.051	0.048
	Conical x = 0 in.	---	---	0.062	0.066	0.059	0.050	---	0.045	---	---
	Conical x = 12 in.	---	---	0.090	0.082	0.074	0.061	---	0.056	---	---

*Figure 4
**Table I

TABLE III (Continued)
d. α = -5 deg, ϕ = 0 deg

Config. *	Flow Conditions**	S/R_N									
		0.784	1.40	3.00	5.00	7.00	10.0	14.9	19.2	23.5	27.8
2.00	Contoured	---	---	0.023	---	---	---	---	---	---	---
	Conical x = 0 in.	0.182	0.037	0.020	---	---	---	---	---	---	---
	Conical x = 12 in.	0.241	0.040	0.025	---	---	---	---	---	---	---
3.10	Contoured	---	---	0.028	0.022	0.019	0.016	---	---	---	---
	Conical x = 0 in.	---	---	0.023	0.020	0.016	0.014	---	---	---	---
	Conical x = 12 in.	---	---	0.032	0.025	0.021	0.015	---	---	---	---
3.11	Contoured	---	---	0.027	0.022	0.020	0.016	---	0.014	---	---
3.12	Contoured	---	---	0.027	0.022	0.017	0.016	---	0.013	0.013	0.011
	Conical x = 0 in.	---	---	0.021	0.018	0.014	0.011	---	0.009	---	---
	Conical x = 12 in.	---	---	0.026	0.023	0.020	0.014	---	0.014	---	---

*Figure 4
**Table I

TABLE III (Concluded)
e. α = -9 deg, ϕ = 0 deg

Config.*	Flow Conditions**	S/R_N									
		0.784	1.40	3.00	5.00	7.00	10.0	14.9	19.2	23.5	27.8
2.00	Contoured	---	---	0.017	---	---	---	---	---	---	---
	Conical x = 0 in.	0.153	0.028	0.013	---	---	---	---	---	---	---
	Conical x = 12 in.	0.210	0.030	0.018	---	---	---	---	---	---	---
3.10	Contoured	---	---	0.021	0.016	0.014	0.011	---	---	---	---
	Conical x = 0 in.	---	---	0.017	0.015	0.012	0.009	---	---	---	---
	Conical x = 12 in.	---	---	0.023	0.017	0.014	0.009	---	---	---	---
3.11	Contoured	---	---	0.019	0.016	0.014	0.010	---	0.009	---	---
3.12	Contoured	---	---	0.021	0.016	0.013	0.011	---	0.009	0.008	0.008
	Conical x = 0 in.	---	---	0.014	0.012	0.010	0.008	---	0.006	---	---
	Conical x = 12 in.	---	---	0.017	0.016	0.014	0.009	---	0.009	---	---

*Figure 4
**Table I

TABLE IV
TABULATION OF SHARP CONE STANTON NUMBERS
a. α = 0 deg, ϕ = 0 deg

Config. *	Flow Conditions**	x′, inches							
		2.53	3.23	3.92	4.97	6.67	8.17	9.67	11.17
3.00	Conical x = 0 in.	0.035	0.030	0.028	0.022	---	---	---	---
	Conical x = 12 in.	0.043	0.038	0.035	0.029	---	---	---	---
3.01	Contoured	0.042	0.040	0.035	0.029	---	---	---	---
3.02	Contoured	0.041	0.037	0.035	0.028	---	0.024	0.024	0.022
	Conical x = 0 in.	0.038	0.036	0.032	0.027	---	0.022	0.021	---
	Conical x = 12 in.	0.046	0.040	0.036	0.030	---	0.024	---	---

*Figure 4
**Table I

TABLE IV (Continued)
b. α = 5 deg, ϕ = 0 deg

Config. *	Flow Conditions**	x′, inches							
		2.53	3.23	3.92	4.97	6.67	8.17	9.67	11.17
3.00	Conical x = 0 in.	0.055	0.049	0.042	0.035	---	---	---	---
	Conical x = 12 in.	0.062	0.053	0.051	0.045	---	---	---	---
3.01	Contoured	0.064	0.060	0.054	0.045	---	---	---	---
3.02	Contoured	0.061	0.055	0.052	0.043	---	0.038	0.036	0.034
	Conical x = 0 in.	0.061	0.057	0.051	0.043	---	0.036	0.032	---
	Conical x = 12 in.	0.069	0.060	0.055	0.046	---	0.038	---	---

*Figure 4
**Table I

TABLE IV (Continued)
c. α = 10 deg, ϕ = 0 deg

Config. *	Flow Conditions**	x′, inches							
		2.53	3.23	3.92	4.97	6.67	8.17	9.67	11.17
3.00	Conical x = 0 in.	0.077	0.069	0.063	0.049	---	---	---	---
	Conical x = 12 in.	0.087	0.075	0.072	0.062	---	---	---	---
3.01	Contoured	0.088	0.082	0.076	0.062	---	---	---	---
3.02	Contoured	0.082	0.074	0.072	0.058	---	0.053	0.048	0.046
	Conical x = 0 in.	0.088	0.081	0.064	0.062	---	0.050	0.046	---
	Conical x = 12 in.	0.097	0.084	0.078	0.067	---	0.055	---	---

*Figure 4
**Table I

TABLE IV (Continued)
d. α = -5 deg, ϕ = 0 deg

Config. *	Flow Conditions**	x′, inches							
		2.53	3.23	3.92	4.97	6.67	8.17	9.67	11.17
3.00	Conical x = 0 in.	0.021	0.018	0.018	0.012	---	---	---	---
	Conical x = 12 in.	0.029	0.025	0.022	0.019	---	---	---	---
3.01	Contoured	0.026	0.023	0.021	0.016	---	---	---	---
3.02	Contoured	0.025	0.023	0.021	0.016	---	0.015	0.014	0.012
	Conical x = 0 in.	0.024	0.023	0.019	0.016	---	0.014	0.012	---
	Conical x = 12 in.	0.029	0.026	0.024	0.019	---	0.015	---	---

*Figure 4
**Table I

TABLE IV (Concluded)
e. α = -9 deg, ϕ = 0 deg

Config.*	Flow Conditions**	x′, inches							
		2.53	3.23	3.92	4.97	6.67	8.17	9.67	11.17
3.00	Conical x = 0 in.	0.015	0.013	0.012	0.008	---	---	---	---
	Conical x = 12 in.	0.020	0.019	0.016	0.015	---	---	---	---
3.01	Contoured	0.019	0.017	0.015	0.011	---	---	---	---
3.02	Contoured	0.017	0.016	0.015	0.011	---	0.010	0.009	0.009
	Conical x = 0 in.	0.015	0.015	0.013	0.011	---	0.009	0.008	---
	Conical x = 12 in.	0.019	0.017	0.016	0.013	---	0.011	---	---

*Figure 4
**Table I

UNCLASSIFIED

Security Classification

DOCUMENT CONTROL DATA - R & D

(Security classification of title, body of abstract and indexing annotation must be entered when the overall report is classified)

1 ORIGINATING ACTIVITY (Corporate author)	2a. REPORT SECURITY CLASSIFICATION
Arnold Engineering Development Center Arnold Air Force Station, Tennessee 37389	UNCLASSIFIED
	2b. GROUP N/A

3 REPORT TITLE

LAMINAR HEAT TRANSFER ON SHARP AND BLUNT TEN-DEGREE CONES IN CONICAL AND PARALLEL LOW-DENSITY FLOW

4 DESCRIPTIVE NOTES (Type of report and inclusive dates)

Final Report - March 1971 to April 7, 1972

5 AUTHOR(S) (First name, middle initial, last name)

D. E. Boylan, ARO, Inc.

6 REPORT DATE	7a. TOTAL NO OF PAGES	7b. NO OF REFS
August 1973	60	23

8a CONTRACT OR GRANT NO	9a. ORIGINATOR'S REPORT NUMBER(S)
b. PROJECT NO	AEDC-TR-73-106
c Program Element 64719F	9b. OTHER REPORT NO(S) (Any other numbers that may be assigned this report)
d.	ARO-VKF-TR-73-47

10 DISTRIBUTION STATEMENT

Approved for public release; distribution unlimited.

11 SUPPLEMENTARY NOTES	12 SPONSORING MILITARY ACTIVITY
Available in DDC	Arnold Engineering Development Center, Air Force Systems Command, Arnold AF Station, Tennessee 37389

13 ABSTRACT The report presents heat-transfer-rate measurements on sharp and blunt 10-deg half-angle cones at angles of attack between -9 and +10 deg in a low-density, hypersonic wind tunnel. Circumferential and longitudinal distributions are presented for cold wall conditions at $18.2 \leq M_\infty \leq 19.9$ and $960 \leq Re_\infty/in. \leq 1250$. The effect of source-like flows was studied by utilizing both conical and contoured expansion nozzles with the same free-stream similarity parameters and model wall temperatures. Comparisons are made to previously published experimental and theoretical results.

DD FORM 1 NOV 65 1473

UNCLASSIFIED

Security Classification

14 KEY WORDS	LINK A		LINK B		LINK C	
	ROLE	WT	ROLE	WT	ROLE	WT
laminar flow						
heat transfer						
cones (sharp and blunt)						
conical bodies						
flow (low-density)						
hypersonic flow						

AFSC
Arnold AFS Tenn